Divergent changes in aerosol optical hygroscopicity and new particle

2	formation induced by heatwaves
3	
4	Yuhang Hao ^{1, a} , Peizhao Li ^{1, a} , Yafeng Gou ¹ , Zhenshuai Wang ¹ , Mi Tian ¹ , Yang Chen ² ,
5 6	Ye Kuang ³ , Hanbing Xu ⁴ , Fenglian Wan ¹ , Yuqian Luo ¹ , Wei Huang ⁵ , Jing Chen ^{1, 6, *}
7	¹ College of Environment and Ecology, Chongqing University, Chongqing 400045,
8	China
9	² Center for the Atmospheric Environment Research, Chongqing Institute of Green
10	and Intelligent Technology, Chinese Academy of Sciences, Chongqing 400714, China
11	³ Institute for Environmental and Climate Research, Jinan University, Guangzhou
12	511443, China
13	⁴ Experimental Teaching Center, Sun Yat-sen University, Guangzhou 510275, China
14	⁵ National Meteorological Center, China Meteorological Administration, Beijing
15	100081, China
16	⁶ Key Laboratory of Three Gorges Reservoir Region's Eco-Environment, Ministry of
17	Education, Chongqing University, Chongqing 400045, China
18	
19	^a These authors contributed equally
2021	Correspondence to: Jing Chen (chen.jing@cqu.edu.cn)
∠ I	Correspondence to. Jing Chen (chen.jing@equ.cau.cii)

Abstract. As a crucial climate-forcing driver, the aerosol optical enhancement factor (f(RH)) is significantly modulated by chemical compositions and the evolution of particle number size distribution (PNSD), e.g., during new particle formation (NPF). However, the mechanisms regulating aerosol optical hygroscopicity during different NPF days, particularly those influenced by heatwaves due to global warming, remain poorly understood. In the extremely hot summer of 2022 in urban Chongqing of southwest China, simultaneous measurements of aerosol optical and hygroscopic properties, PNSD, and bulk chemical compositions were conducted. Two distinct types of NPF were identified: the ones with relatively polluted period (NPF_P) and clean cases during heatwave-dominated period (NPF_{C, HW}). Compared to the NPF_P events, NPF_{C, HW} occurred approximately one hour earlier and the subsequent growth was prolonged, accompanied by a smaller aerosol effective radius (Reff) and lower formation/growth rate during heatwaves. This agreed with the concurrently increased aerosol hemispheric backscattering fraction and scattering Ångström exponent. f(RH) was generally higher on NPF days in comparison to that for non-event cases in both periods. Moreover, heatwave-induced stronger photooxidation may intensify the formation of more hygroscopic secondary components, as well as the atmospheric aging/subsequent growth of both pre-existing and newly formed particles, thereby enhancing f(RH) especially during NPF_{C, HW} days. The promoted f(RH) and lowered Reff could synergistically elevate the aerosol direct radiative forcing, specifically under persistent heatwave conditions. Further in-depth exploration on molecular-level characterizations and aerosol radiative impacts of both direct and indirect interactions during weather extremes (e.g., heatwaves) with the warming climate are recommended.

46

47

48

49

22

23

24

25

26

27

28

29

30

31

32

33

34

35

36

37

38

39

40

41

42

43

44

45

1 Introduction

Weather extremes (e.g., heatwaves) have become more and more frequent and intense largely due to the global climate change, and the heatwave-driven

environmental, climatic, and health effects have garnered widespread attention (Hauser et al., 2016; Sun et al., 2016). The China Climate Bulletin 2022 confirmed that the national average temperature reached an unprecedented high level since 2012 (China Meteorological Administration, 2022), and the risk of heatwaves in China will persist and potentially intensify in the future (Guo et al., 2016; Li et al., 2017). Extreme heatwave events could pose significant threats to human health, the survival of organisms, agriculture, and socio-economic activities (e.g., power supply restrictions) (Anderson and Bell, 2011; Ma et al., 2021; Su, 2021). Moreover, heatwaves can trigger natural disasters such as droughts and wildfires, affecting social stability (Sharma and Mujumdar, 2017).

50

51

52

53

54

55

56

57

58

59

60

61

62

63

64

65

66

67

68

69

70

71

72

73

74

75

76

77

78

79

Heatwaves could also affect the atmospheric physical and chemical processes by modulating ambient meteorological conditions. Specifically, extremely high temperature weather is typically characterized by a combination of intensified solar radiation with elevated temperature and low humidity levels. This could significantly affect the formation and evolution of secondary aerosols in the atmosphere (Bousiotis et al., 2021; Hamed et al., 2011; Kurtén et al., 2007), given that the air temperature is crucial for chemical reactions (Xu et al., 2011). New particle formation (NPF) serves as a crucial source of atmospheric particulate matter and plays a significant role in the secondary transformation processes in the atmosphere (Zhu et al., 2021). Generally, NPF involves the initial formation of thermodynamically stable clusters from condensable vapors (e.g., ammonia, sulfuric acid, and organic precursor gases) and subsequent growth of the formed clusters, eventually reaching detectable sizes or even larger dimensions (Kerminen et al., 2018; Kulmala et al., 2003, 2012). Over time, these newly formed particles have the potential to serve as cloud condensation nuclei (CCN), thereby impacting the global climate (Salma et al., 2016). NPF events normally introduce a sharp increase in the number concentration of nucleation mode particles within a short time, altering the particle number size distribution (PNSD). These variations in PNSD likely influence intrinsic physicochemical properties of aerosols, such as the optical hygroscopicity (Chen et al., 2014; Titos et al., 2016; Zhao et al., 2019).

Aerosol hygroscopicity plays a critical role in the atmospheric environment and climate change, given the complex interaction between aerosol particles and water vapor (Zhao et al., 2019; Zieger et al., 2011). Water uptake by aerosols not only alters the particle size and composition (e.g., as reflected in the aerosol refractive index) but also impacts aerosol scattering efficiency, which further contributes to the uncertainty in aerosol radiative forcing estimation (Titos et al., 2016, 2021). The aerosol optical hygroscopicity parameter, f(RH), defined as the ratio of the scattering coefficient at a certain RH to that of the dry condition, was widely used to describe the aerosol scattering enhancement through water uptake (Covert et al., 1972; Titos et al., 2016; Zhao et al., 2019). Numerous studies have demonstrated that f(RH) is influenced by the size distribution, in addition to particle chemical composition (Chen et al., 2014; Kuang et al., 2017; Petters and Kreidenweis, 2007; Quinn et al., 2005). There is currently limited research on the variations in aerosol optical hygroscopicity during NPF days despite significant changes in aerosol size distributions and chemical compositions, partly due to that newly formed particles insignificantly affect the optical properties of aerosols (Kuang et al., 2018). However, previous studies have observed the enhancement in aerosol hygroscopicity (Cheung et al., 2020; Wu et al., 2015, 2016) and extinction coefficients (Shen et al., 2011; Sun et al., 2024) during the subsequent growth of NPF. It is suggested that the influence of NPF on aerosol hygroscopicity was likely due to changes in aerosol chemical composition at different stages of NPF events (Cheung et al., 2020), whereas the subsequent particle growth associated with NPF events can significantly affect particle hygroscopicity as well (Wu et al., 2016). Although previous studies showed the dependences of aerosol hygroscopicity on chemical composition (Petters and Kreidenweis, 2007; Titos et al., 2016; Zhao et al., 2019) (e.g., the variation in composition of precursor species during NPF events), it is important to acknowledge that the utilized chemical compositions of NPF were either from PM_{2.5} or PM₁ bulk data. This may differ from the corresponding composition of newly formed ultrafine particles primarily in the nucleation and Aitken modes, further introducing bias in exploring the impacts of NPF and subsequent growth on aerosol optical hygroscopicity. Hence, more

80

81

82

83

84

85

86

87

88

89

90

91

92

93

94

95

96

97

98

99

100

101

102

103

104

105

106

107

108

comprehensive investigations on the influencing mechanisms of aerosol optical hygroscopicity from different perspectives are required, e.g., for the aspects of the evolution of particle size distribution in modulating aerosol optical and hygroscopic properties (Tang et al., 2019; Zhao et al., 2019). Additionally, field observations on f(RH) under extreme weather conditions (e.g., heatwaves) are rather scarce, largely hindering our understanding of how weather extremes (e.g., extremely high temperature) influence the optical hygroscopic properties of aerosols. This knowledge gap further impedes comprehensive understanding of the aerosol water uptake property and resulted effects on air quality and the climate under varied synoptic conditions.

During the summer of 2022, a rare heatwave event raged throughout China, especially the Sichuan-Chongqing region of southwest China (Chen et al., 2024; Wang et al., 2024), with the daily maximum temperature exceeding 40 °C lasted for 29 days observed at Beibei meteorological station in Chongqing (Hao et al., 2023). This persistent heatwave not only impacted residents' daily lives significantly, but also affected the aerosol optical and hygroscopic properties likely through changed aerosol physicochemical characteristics and relevant atmospheric processing during the period. In this study, a field observation was conducted by using a combination of a home-built humidified nephelometer system and a scanning mobility particle sizer (SMPS), along with the total suspended particle (TSP) filter sampling. A main goal of this study is to investigate the influence of heatwaves on both aerosol optical hygroscopicity and the NPF with subsequent growth events, along with the related discrepancies. Furthermore, we aimed to explore the mechanisms behind the variability in f(RH) under different meteorological conditions and diverse NPF events. This study will further enrich insights into the potential environmental impacts due to variations in the aerosol optical hygroscopicity and size distribution, specifically under weather extremes (e.g., heatwaves) with the changing climate.

2 Data and Methods

138

139

140

141

142

143

144

145

146

147

148

149

150

151

152

153

154

155

156

157

158

159

160

161

162

163

164

165

2.1 Field observation

A continuous field observation on aerosol optical, hygroscopic and chemical properties was carried out from July 29 to August 19, 2022. The detailed description of the observation site is available in Supporting Information, S1. During the observation period, urban Chongqing suffered a rare heatwave (Fig. S1; Chen et al., 2024; Wang et al., 2024), which significantly affected the local transportation and industrial activities (Hao et al., 2023). China Meteorological Administration (CMA) defines heatwaves as three or more consecutive days with daily maximum temperature (T_{max}) above 35 °C (http://www.cmastd.cn/standardView.jspx?id=2103; Guo et al., 2016; Sun et al., 2014; Tan et al., 2007). Since no unified definition of heatwaves worldwide, the whole study period was categorized into two stages according to CMA's criteria of the daily T_{max} records and the Excess Heat Factor (EHF) metric proposed by Nairn and Fawcett (2014) (Fig. S2a): (1) the normally hot period from 29 July to 6 August (marked as P1); (2) the heatwave-dominated period from August 7-19 (marked as P2) characterized with the consistently occurrence of T_{max} exceeding 38 °C (approximately the last 25th percentile of temperature records for the whole observation period; Fig. S2b).

2.2 Instrumentation and methods

2.2.1 Measurements of aerosol optical hygroscopicity

The humidified nephelometer system, consisting of two three-wavelength (i.e., 450, 525, and 635 nm) nephelometers (Model Aurora 3000, Ecotech Inc.) and a humidification unit, was used to determine the aerosol light scattering enhancement factor, f(RH). Ambient air was firstly dried through a Nafion dryer (model MD-700, Perma Pure LLC) to ensure RH <35%, then split into two streams for both dry and humidified nephelometers operated in parallel. The flowrate for each nephelometer was 2.6 LPM. The aerosol scattering (σ_{sca} , λ) and backscattering coefficients (σ_{bsca} , λ) were detected in a dry state (RH <35%) and at a controlled RH level of 85 \pm 1%,

respectively, with the humidification efficiency regulated automatically by a temperature-controlled water bath. More details on the home-built humidified nephelometer system are available in Kuang et al. (2017, 2020) and Xue et al. (2022).

Hence, f(RH) could be calculated as the ratio of the aerosol scattering coefficient at a predefined RH ($\sigma_{sca, RH}$) to the dry ($\sigma_{sca, dry}$) state, i.e., $f(RH) = \sigma_{sca, RH} / \sigma_{sca, dry}$ (Covert et al., 1972). In this study, the f(RH) discussed is mainly targeted for the 525 nm wavelength, unless otherwise specified. More information about the measurement of humidified nephelometer system was illustrated in Sect. S2 of the supplement.

In additional to f(RH), aerosol optical parameters, such as scattering Ångström exponent (SAE; Schuster et al., 2006) and hemispheric backscattering fraction (HBF; Collaud Coen et al., 2007), were calculated as below:

$$SAE_{\lambda 1/\lambda 2} = \frac{-\ln(\sigma_{sea, \lambda 1}/\sigma_{sea, \lambda 2})}{\ln(\lambda 1/\lambda 2)}$$
 (1)

178
$$HBF_{\lambda} = \frac{\sigma_{bsca, \lambda}}{\sigma_{sca, \lambda}}$$
 (2)

where $\sigma_{sca, \lambda}$ and $\sigma_{bsca, \lambda}$ represent the aerosol scattering and backscattering coefficients at a specific wavelength λ (e.g., $\lambda 1$, $\lambda 2$), respectively.

Both HBF and SAE reflect crucial optical properties of aerosols, e.g., an elevated HBF (or SAE) generally signifies a higher concentration (or a smaller particle size) of fine particles within the aerosol population (Jefferson et al., 2017; Kuang et al., 2017; Luoman et al., 2019). The HBF and SAE discussed in this study are targeted for the dry condition, unless otherwise specified. Based on the measurements with the humidified nephelometer system, the equivalent aerosol liquid water content (ALWC) and the corresponding fraction of ALWC (f_W) can also be obtained (Kuang et al, 2018; see Sect. S2 of the supplement).

The SMPS-measured concurrent particle number size distributions were further utilized to calculate the aerosol effective radius (R_{eff}) and representative parameters for NPF events, e.g., the formation rate (FR) and growth rate (GR) of new particle, condensation sink (CS) and coagulation sink (CoagS) (Dal Maso et al., 2005; Kulmala et al., 2012). More details are provided in the supplement (Sect. S5).

Results of the offline chemical analysis with TSP filter samples are provided in Sect. S3 and Fig. S3. It should be noted that certain secondary organics and crustal elements (e.g., Ca²⁺, Mg²⁺) that could exhibit a broader size distribution may contribute to the observed discrepancy in the total mass concentration between the 24-h TSP samples and daily mean PM_{2.5} (of similar temporal variations; Fig.S3) (Duan et al., 2024; Kim et al., 2020; Xu et al., 2021). Nonetheless, previous studies reported that key components such as SNA (i.e., SO₄²⁻, NO₃⁻, and NH₄⁺) and primary organics of PM_{2.5} (or PM₁₀) were predominantly concentrated within the submicron size range (An et al., 2024; Bae et al., 2019; Chen et al., 2019; Duan et al., 2024; Kim et al., 2020; Xu et al., 2024). While the use of TSP samples contains some uncertainties, the bulk chemical information remains reasonable for characterizing the optical and hygroscopic properties of PM_{2.5}. The descriptions of simultaneous meteorological and air quality data can be found in Sect. S4, and the 48-h backward trajectory analysis was given in Sect. S5 of the supplement.

2.2.2 Determination of the aerosol direct radiative forcing (ADRF) enhancement factor

Given the high sensitivity of aerosol optical properties (e.g., f(RH)) to the changes in RH under real atmospheric conditions, the influence of RH, or rather the aerosol hygroscopicity, on ADRF can be quantitatively estimated with the radiative transfer model by the following equation (Chylek and Wong, 1995; Kotchenruther et al., 1999; L. Zhang et al., 2015):

$$\Delta F_R(RH) = -(S_0/4) \times [T_a^2 \times (1 - A_C)] \times [2 \times (1 - R_s)^2 \times \beta(RH) \times \tau_s - 4 \times R_s \times \tau_a]$$
 (3)

where S_0 is the solar constant, T_a is the atmosphere transmittance, A_C is the fractional cloud amount, R_s is the albedo of the underlying surface, $\beta(RH)$ is the upscattering fraction at a defined RH, τ_s and τ_a are the optical thicknesses of the aerosol layer due to light scattering and light absorption, respectively, which can be expressed as follows (Kotchenruther et al., 1999):

221
$$\tau_s = M \times \alpha_s \times f(RH), \tau_a = M \times \alpha_a \tag{4}$$

where M is the column burden of aerosol (unit: gm⁻²), α_s is the mass scattering efficiency (MSE), and α_a is the mass absorption efficiency (MAE). The direct radiative forcing is usually calculated with the assumption that the absorption enhancement is negligible, in comparison to the aerosol scattering enhancement (Xia et al., 2023).

Hence, the dependence of ADRF on RH (i.e., $f_{RF}(RH)$) can be estimated by equation (5) (Chylek and Wong, 1995; Kotchenruther et al., 1999; L. Zhang et al., 2015):

230
$$f_{RF}(RH) = \frac{\Delta F_R(RH)}{\Delta F_R(dry)} = \frac{(1 - R_s)^2 \times \beta(RH) \times \alpha_s \times f(RH) - 2 \times R_s \times \alpha_a}{(1 - R_s)^2 \times \beta(dry) \times \alpha_s \times f(dry) - 2 \times R_s \times \alpha_a}$$
 (5)

where the constant parameters used were $R_s = 0.15$, $\alpha_a = 0.3 \text{ m}^2 \cdot \text{g}^{-1}$ (Hand and Malm, 2007; Fierz-Schmidhauser et al., 2010). It should be noted that the assumed constant α_a might introduce some uncertainty in the calculated $f_{RF}(RH)$, given the fact that the contribution of absorption by brown carbon was unknown, although the mass fraction of BC in TSP remained almost constant (i.e., $4.6\% \pm 1.1\%$, Fig. S3) during the observation period. The parameter α_s was calculated by dividing $\sigma_{sca, 525}$ in the dry condition by the mass concentration of PM_{2.5} (i.e., $\alpha_s = \sigma_{sca, 525}$ / PM_{2.5}). β could be calculated empirically from the measured HBF: $\beta = 0.0817 + 1.8495 \times \text{HBF} - 2.9682 \times \text{HBF}^2$ (Delene and Ogren, 2002).

3 Results and discussion

3.1 Overview of the aerosol optical hygroscopicity and PNSD measurements

Figure 1 displayed the time series of the measured aerosol scattering coefficients, f(RH), PNSD, and the corresponding meteorological conditions and air pollutants during the study period. A sharp decrease in aerosol scattering coefficients and PM_{2.5}, accompanied with the continuous excellent visibility over 20 km was observed after August 6, indicating a markedly cleaner environment during P2 in comparison to P1 in summer 2022 of Chongqing. This could be largely attributed to the reduction in anthropogenic emissions (e.g., NO₂, CO, except SO₂) from limited outdoor activities

influenced by the heatwaves in P2, as well as partly suspended industries and transportation to alleviate the power shortage issue (Chen et al., 2024). Notably, the increased wind speed and enhanced mixing layer height (MLH) also enabled a more favorable atmospheric diffusion condition in P2, facilitating the dilution of surface air pollutants (Zhang et al., 2008). However, a higher mass concentration of SO₂ was observed in the P2 period, likely due to a surge in electricity demand and resulted higher emissions from power plants operating almost at full capacity during the heatwave (Su, 2021; Teng et al., 2022). Moreover, significant discrepancies in the aerosol optical and hygroscopic properties were observed under different synoptic conditions (Table S2). Both HBF and SAE were higher during the P2 period, aligning with the smaller R_{eff} (Table S2). The f(RH) was found to be relatively higher (p < 0.05) in heatwave days, with the mean values of 1.61 ± 0.12 and 1.71 ± 0.15 during the P1 and P2 periods, respectively. Differently, ALWC was more abundant during the normally hot P1 period than the heatwave-dominated P2 period. This is likely due to that the derivation algorithm of ALWC utilized in this study (Kuang et al., 2018) was partly dependent on (e.g., positively correlated) the dry aerosol scattering coefficient, or rather the aerosol volume concentration in the dry condition (refer to Sect. S3 and Fig. S11 of the supplement). The mean $\sigma_{sca, 525}$ for P2 was about 46.8% of that for the P1 period, and the corresponding mean level of ALWC was approximately 55.8% of that for P1. This partly agrees with the stronger aerosol optical hygroscopicity with a marginally higher f_W during the P2 period, highlighting a complex interaction between the optical enhancement and aerosol physicochemical properties.

249

250

251

252

253

254

255

256

257

258

259

260

261

262

263

264

265

266

267

268

269

270

271

272

273

274

275

276

277

278

The particle number size distribution data suggested that NPF events appeared in about half the number of observation days (Fig. 1i), with an overall occurrence frequency of 52.4% (Fig. S4a). This suggests the rather frequent summer NPF events in Chongqing, notably higher than those observed in other regions of the world, e.g., Beijing (16.7%, Deng et al., 2020; ~20%, Wang et al., 2013), Dongguan (4%, Tao et al., 2023), Hyytiälä (<40%, Dada et al., 2017) and LiLLE (<20%, Crumeyrolle et al., 2023). Moreover, the frequent NPF events during heatwaves formed substantially ultrafine particles that are of less contribution to aerosol optical properties in

comparison to large particles, partially explaining the significantly lower levels of total scattering coefficients observed during the P2 period. It should be noted that the hourly $\sigma_{sca, 525}$ values during the P2 period were exclusively below 100 Mm⁻¹ (approximately the last 10^{th} percentile of $\sigma_{sca, 525}$ data, regarded as the threshold value of relatively polluted cases; Fig. S2c), suggesting a much cleaner environment compared to the relatively polluted P1 period. Correspondingly, NPF events occurring during the relatively polluted P1 period (as detailed in section 3.2) were defined as NPF_P, while cases during the cleaner and heatwave-dominated P2 period were classified as NPF_{C, HW}.

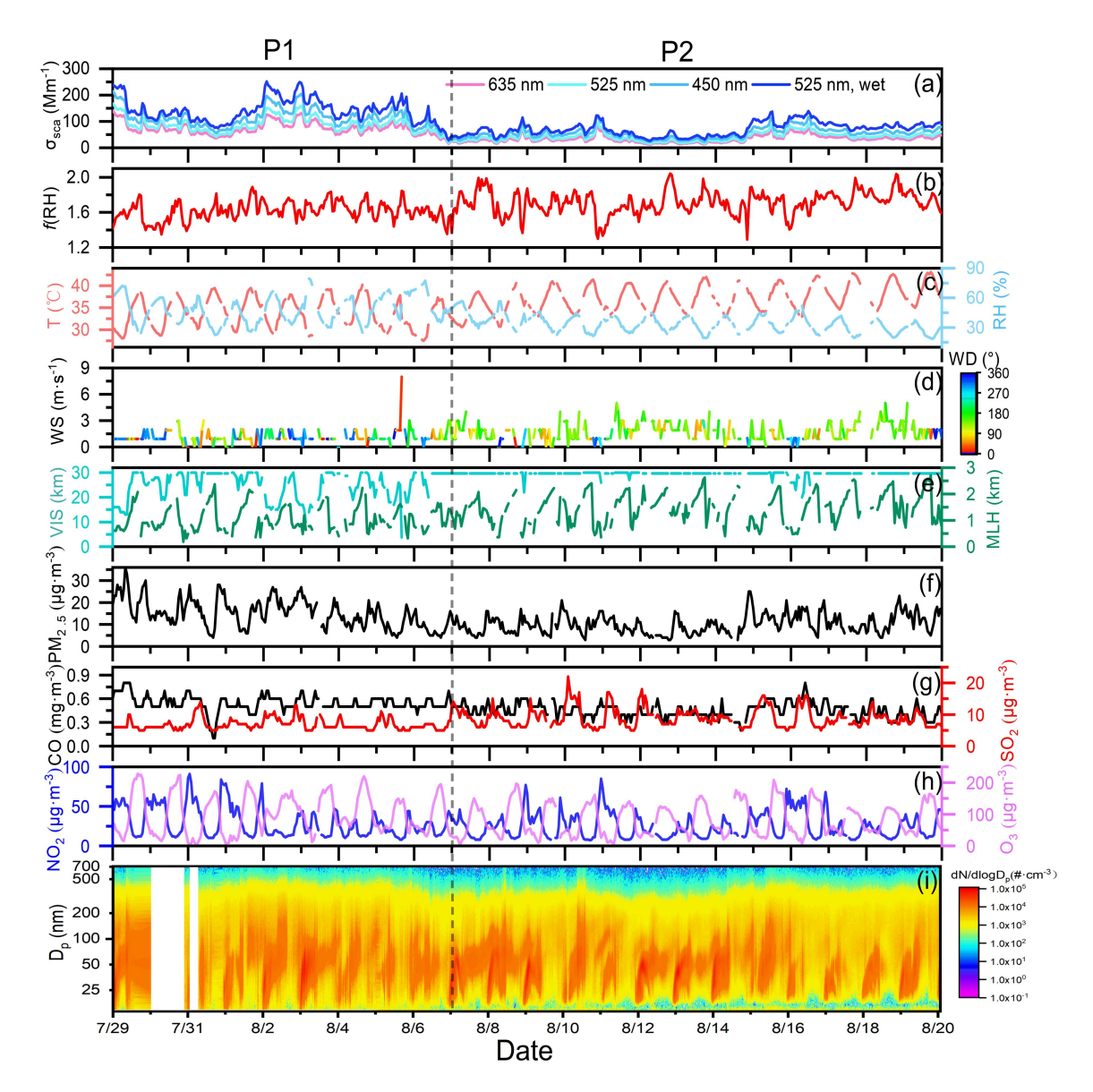


Figure 1. Time series of the measured aerosol scattering coefficients, f(RH), meteorological conditions, air pollutants, and particle number size distribution during the study period.

3.2 Characteristics of NPF events in different periods

Aside from gaseous precursors (e.g., SO₂, volatile organic compounds), meteorological conditions also play a key role in the occurrence of NPF events. In brief, NPF events are more likely to appear under sunny and clean conditions (Bousiotis et al., 2021; Crumeyrolle et al., 2023; Deng et al., 2021; Wang et al., 2017). The backward trajectory analysis revealed that the southerly breeze was predominant during the study period (Fig. S4b). Although the surface wind vector slightly varied between the P1 and P2 periods, this consistency in air mass origins suggests that some other factors (e.g., changes in environmental conditions and emissions of gaseous precursors under heatwaves) could have played a crucial role in modulating NPF events. To further explore the characteristics of NPF events in different periods, the time-averaged diurnal variations of meteorological parameters and air pollutant concentrations during both NPF events and non-event days are presented in Fig. 2.

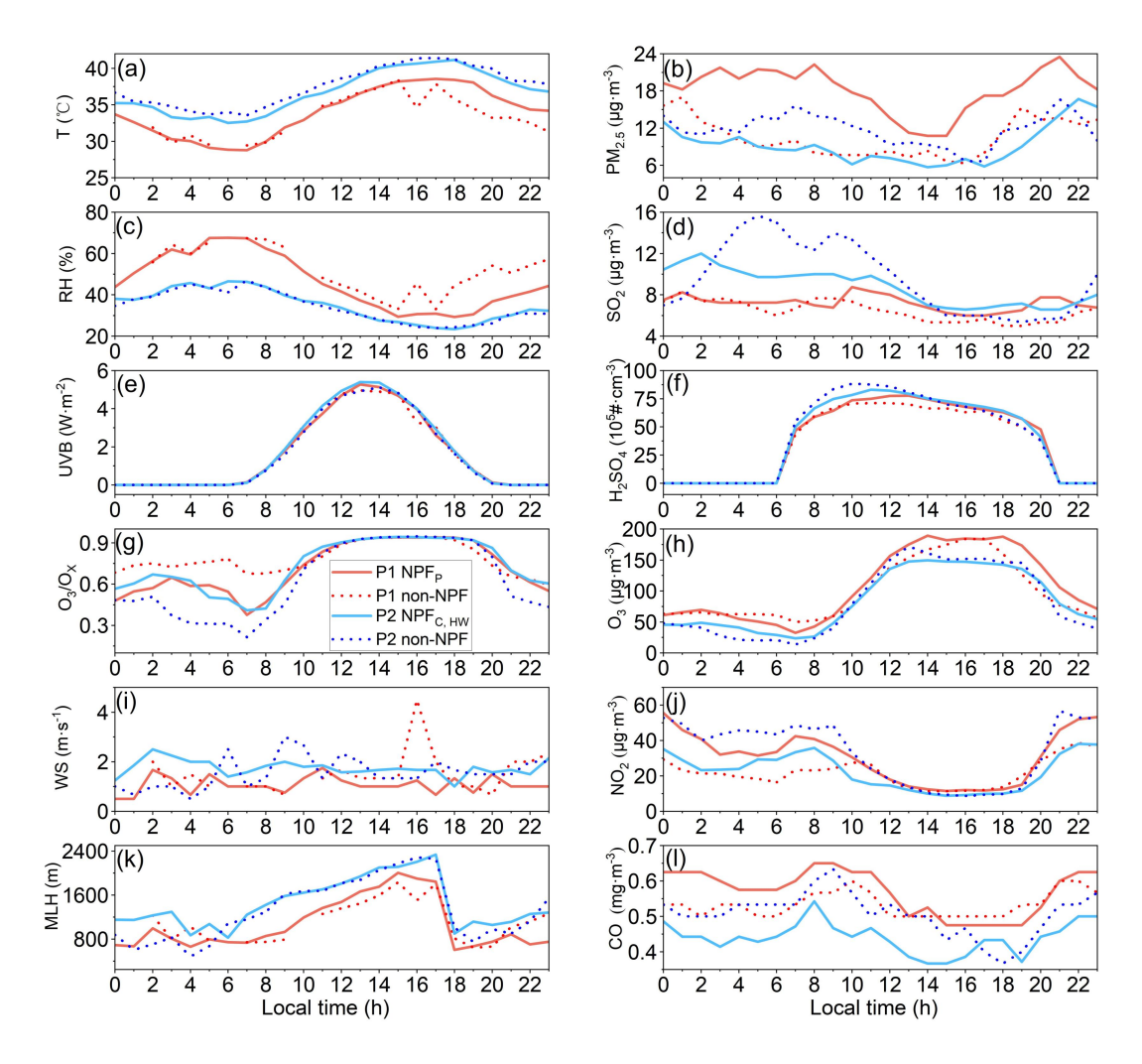


Figure 2. Diurnal variations of temperature (a), PM_{2.5} mass loading (b), RH (c), SO₂ (d), UVB (e), H₂SO₄ (f), O₃/O_X (g), O₃ (h), WS (i), NO₂ (j), MLH (k) and CO (l) during P1 (red) and P2 (blue) NPF days (solid line), as well as the corresponding non-event days (dash line).

As stated in Sect.3.1, NPF events during the P1 period tended to occur in relatively polluted environments compared to that of P2 NPF_C, HW events, as evidenced by the frequent occurrence of σ_{sca} , 525 >100 Mm⁻¹, increased air pollutant concentrations and lower visibility levels during P1 (Table S2, Fig. 1). Additionally, the mean CS of the NPF_P events was above 0.015 s⁻¹ (Table S2), which could be considered as the "polluted" NPF cases (Shang et al., 2023). On P2 NPF_C, HW days, the overall mean σ_{sca} , 525 was 33.2 \pm 11.7 Mm⁻¹, decreased by 68.0% (39.3%) in comparison to that for P1 NPF_P days (P2 non-event days). In addition, the mean PM_{2.5} concentration was even lower than 10.0 μ g·m⁻³, and the corresponding visibility level

was almost maintained at 30 km (Fig. 1e). All the above implies that the P2 NPF_{C, HW} events were generally accompanied with a much cleaner environment. It is notable that the increase in SO₂ concentration after 9:00 LT (Fig. 2d), along with the significant decrease in PM_{2.5} mass loadings after 8:00 LT during P1 NPF_P events (Fig. 2b), likely favored the occurrence of NPF events. The higher gas-phase sulfuric acid (i.e., H₂SO₄, as estimated with the UVB and SO₂ concentration, Lu et al., 2019, Sect. S4) on the same NPF days (Fig. 2f), further suggesting that sulfuric acid concentration was a critical factor for the occurrence of P1 NPF_P events.

319

320

321

322

323

324

325

326

327

328

329

330

331

332

333

334

335

336

337

338

339

340

341

342

343

344

345

346

347

348

The diurnal evolutions of meteorological conditions (e.g., T, RH, MLH) for NPF events were distinct between P1 and P2 periods, although relatively insignificant differences were observed for both NPF days and non-event days within a same period (Fig. 2). This likely suggests that meteorological factors might not be the predominant determining factor of NPF occurrence during the heatwaves of 2022 summer in urban Chongqing, while NPF could be accompanied with quite different meteorological conditions depending on gaseous precursors and preexisting condensation sinks. For instance, the NPF_{C, HW} events were typically of clean-type NPF, characterized with lower background aerosol loading, higher temperature and favorable atmospheric dispersion capacity with the higher MLH. However, it is reported that excessive heat can increase the evaporation rate of critical acid-base clusters during the nucleation process and reduce the stability of initial molecular clusters (Bousiotis et al., 2021; Kurtén et al., 2007; Zhang et al., 2012), in line with a recent study that NPF events were weaker during heatwayes in Siberian boreal forest due to the unstable clusters (Garmash et al., 2024). On the other hand, the emission rate of biogenic VOCs (BVOCs, e.g., isoprene, monoterpene) from nearby plants and trees would decrease when temperature exceeded around 40 °C (Guenther et al., 1993; Pierce and Waldruff, 1991), despite that BVOCs plays a key role in the nucleation mechanism of NPF (Wang et al., 2017; Zhang et al., 2004). Hence, the even higher temperature (e.g., T >40 °C) likely suppressed the nucleation processes and the subsequent growth of nucleation mode particles on P2 non-event days (Fig. S6b2), in spite of higher concentrations of SO₂ and H₂SO₄.

To further investigate the effect of heatwave on NPF events, the diurnal variations of PNSD, R_{eff} and particle mode diameter (D_{mode}) were shown in Fig. S6. Aerosol number and volume concentrations, as well as Reff, for different modes were illustrated in Fig. S7, and the relationship between temperature and the duration of NPF events was displayed in Fig. S8. The NPF events under heatwaves usually initiated earlier (Fig. S8), with the number concentration of nucleation mode particles (N_{Nuc.}) in P2 NPF_{C, HW} cases peaked about an hour earlier in comparison to NPF_P days (Fig. S7a). The D_{mode} on P2 NPF_{C, HW} days also reached its minimum earlier than that on P1 NPF_P days (Fig. S6). Since the sunrise and sunset time did not significantly vary within the study period (i.e., less than a half hour discrepancy), heatwaves likely provided more favorable conditions (e.g., enhanced volatile gaseous emissions, low RH; Bousiotis et al., 2021; Hamed et al., 2007; Wang et al., 2024) for the occurrence of NPF events in urban Chongqing. This is supported by the earlier start time of NPF_C, HW corresponding to higher temperature ranges (Fig. S8). Furthermore, the end time of subsequent particle growth during P2 period was even later (i.e., ~ 21:00 LT) than that of P1 cases (Fig. S8). Given that the growth rates of new particles were generally lower during P2 NPF_{C, HW} events (Table S2), these explosively formed new particles could persist longer in the warmer atmosphere and probably undergo aging processes with a relatively higher oxidation degree. This is supported by the commonly higher ratios of secondary organic carbon (SOC) to organic carbon (OC) (i.e., SOC/OC >0.5) during the NPF_{C, HW} days (Fig. S3b). In addition, aerosol R_{eff} was significantly smaller on the NPF_{C. HW} days under heatwave conditions. The R_{eff} and D_{mode} nearly kept at a same level below/approaching 50 nm during the subsequent growth on the P2 NPF_C, HW days, while the Reff was generally above 50 nm and larger than D_{mode} for both P1 NPF_P cases and non-event days (Fig. S6). The diurnal patterns of aerosol volume concentrations for different size modes were similar to that of aerosol number concentrations during NPF events (Fig. S7b1-b3). However, both the Reff of Aitken mode particles (R_{Ait.}) and accumulation mode particles (R_{Acc.}) were smaller during P2 NPF_{C, HW} events than that of P1 NPF_P events (Fig. S7c2-c3), which may further influence size-dependent aerosol optical and hygroscopic properties (e.g., $\sigma_{sca, 525}$,

349

350

351

352

353

354

355

356

357

358

359

360

361

362

363

364

365

366

367

368

369

370

371

372

373

374

375

376

377

HBF, SAE, f(RH)). The decrease in R_{Ait.} and R_{Acc.} during heatwaves could be attributed to three factors: (1) evaporation of the outer layer of particles and unstable 380 clusters due to heatwaves (Bousiotis et al., 2021; Cusack et al., 2013; Deng et al., 2020; Garmash et al., 2024; Li et al., 2019); (2) lower FR and GR of particles under the cleaner environment (Table S2); (3) reduced emissions of larger primary particles 384 during the P2 period.

379

381

382

383

385

386

387

388

389

390

391

392

393

394

395

396

397

398

399

400

3.3 Characteristics of the aerosol optical and hygroscopic properties on different types of NPF days

Diurnal variations of the aerosol optical and hygroscopic parameters during different NPF days were shown in Fig. 3, and the corresponding results for non-event days can refer to Fig. S9. Generally, $\sigma_{sca, 525}$ possessed a similar bimodal diurnal pattern to that of the accumulation mode aerosol volume concentration (V_{Acc.}) (Fig. S7b3), as supported by the positive correlation between $\sigma_{sca, 525}$ and SMPS-measured aerosol volume concentration (Fig. S11). This is also consistent with the Mie theory, with a stronger increase in the scattering efficiency for accumulation mode particles (Titos et al., 2021). The diurnal pattern of $\sigma_{sca, 525}$ also varied distinctly between different NPF days. Specifically, a minor peak of $\sigma_{sca, 525}$ around 12:00 LT (Fig. 3a) was influenced by the newly formed particles during P2 NPF_{C, HW} events, which contributed more significantly to the aerosol number and volume concentrations within 100 nm size ranges in markedly clean environments (Fig. S5c1, c2). Instead of a noontime peak, $\sigma_{sca, 525}$ was observed with an early peak around the morning rush hours and a maximum value similarly occurred at the nighttime on P1 NPF_P days.

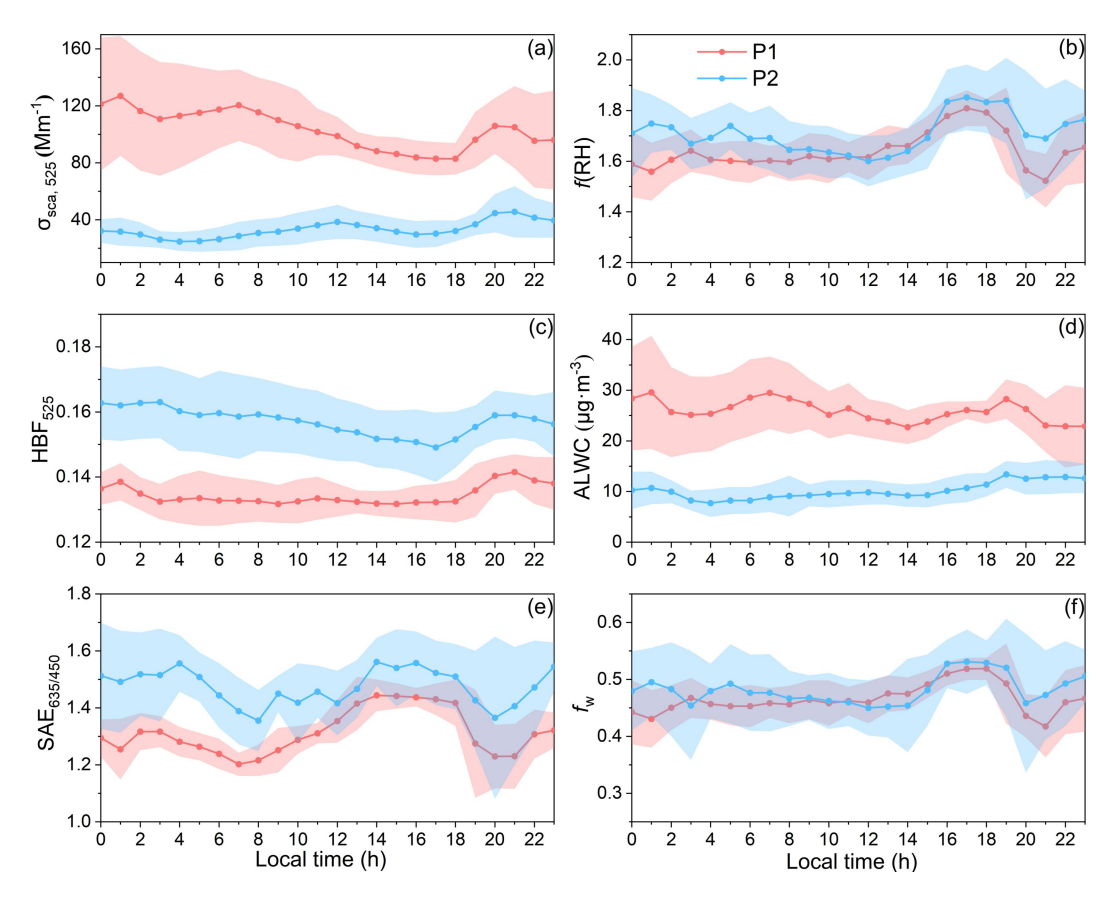


Figure 3. Diurnal variations of $\sigma_{sca, 525}$ (a), f(RH) (b), HBF₅₂₅ (c), ALWC (d), SAE_{635/450} (e) and f_W (f) on NPF days during P1 (red line) and P2 (blue line) periods. The shaded areas stand for the corresponding $\pm 1\sigma$ standard deviations.

Both HBF and SAE on P2 NPF_{C, HW} days were significantly higher than that of P1 NPF_P cases (Fig. 3c, e), largely due to the smaller R_{eff} observed during heatwave-dominated period (Table S2). Moreover, the correlation between HBF (or SAE) and particle size in each mode was weaker on NPF days than on non-event days, especially for NPF_{C, HW} days (Fig. S13). A strongest negative correlation was found between HBF and R_{eff} of the accumulation mode in comparison to other modes, highlighting that HBF is more sensitive to the size distribution of accumulation mode particles (Collaud Coen et al., 2007). Given that NPF would largely enhance the abundance of both nucleation and Aitken mode aerosols, no significant variation in HBF was observed during the daytime due to the weakened correlation between HBF and R_{Acc.} of NPF events. SAE is commonly used as an indicator of particle size distribution, almost decreasing monotonously with the increase of aerosol size within 1 μm (Kuang et al., 2017, 2018; Luoma et al., 2019). Accordingly, SAE decreased

over the morning and evening rush hours when coarse particles (e.g., aged particles, road dust, automobile exhaust) generated during anthropogenic activities, accompanied with an increase in CO that is taken as the proxy for primary emissions (Fig. 2l) (Yarragunta et al., 2020). On the contrary, the abundant ultrafine particles formed during NPF events led to a continuous increase in SAE during the day.

418

419

420

421

422

423

424

425

426

427

428

429

430

431

432

433

434

435

436

437

438

439

440

441

442

443

444

445

446

447

f(RH) exhibited a similar diurnal pattern on the P1 and P2 NPF days (Fig. 3b). During the daytime, f(RH) remained relatively stable and gradually increased until peaking around 16:00-18:00 LT, with a generally higher f(RH) particularly after 15:00 LT during P2 NPF_{C. HW} days than that of P1 cases. The insignificant fluctuation of relatively lower f(RH) levels before the noon could be attributed to the continuous development of the mixing layer (Fig. 2k), leading to an efficient mixing of particles in the nocturnal residual layer with anthropogenic emissions near the ground. Additionally, photochemical reactions in the afternoon facilitated the formation of more hygroscopic secondary aerosols with a higher oxidation level (Liu et al., 2014; R. Zhang et al., 2015). The diurnal patterns of O₃ and the O₃/O_X ratio (i.e., an indicator of atmospheric oxidation capacity, where $O_X = O_3 + NO_2$, Tian et al., 2021) also showed similar trends (Fig. 2g, 2h). The presence of black carbon (BC) mixed with organic compounds (e.g., from traffic emissions and residential cooking activities) explained the rapid decrease in f(RH) during the evening rush hours (Liu et al., 2011). Furthermore, the daily mean f(RH) for NPF days was higher than that of non-event days (Table S2), particularly after the ending of NPF events around 12:00 LT. Given that newly formed particles were too small to significantly impact the total light scattering (Fig. S10a), this indicates that the atmospheric conditions conducive to the occurrence of NPF may promote further growth (e.g., via photooxidation or atmospheric aging processes) of pre-existing particles and newly formed ones, leading to enhanced aerosol optical hygroscopicity as clued from the concurrent variations of ALWC and fw in urban Chongqing during hot summer (Asmi et al., 2010; Wang et al., 2019; Wu et al., 2016). The diurnal pattern of ALWC closely mirrored the variation in $\sigma_{\text{sca, 525}}$, while f_{W} followed the similar evolution of f(RH). This suggests that ALWC was more sensitive to changes in the aerosol volume concentration, as determined by

the corresponding retrieval algorithm (Kuang et al., 2018). The f_W levels were slightly higher during NPF days in comparison to that of non-event days (Table S2). This difference was more pronounced in the afternoon of NPF days (e.g., even exceeded 50%; Fig. 3f), verified the enhancement of aerosol hygroscopicity during the subsequent growth and atmospheric aging of both pre-existing and newly formed particles.

3.4 Heatwave-induced divergent changes in aerosol optical hygroscopicity

To further explore the impacts of heatwaves on *f*(RH) during diverse NPF events, data mainly within the time window of 08:00-22:00 LT (i.e., typically covered the complete process of NPF and subsequent growth, while excluded higher RH conditions at night) were utilized for the following discussion.

A positive correlation between *f*(RH), R_{eff} and the volume fraction of accumulation mode particles (VF_{Acc.}) was found on non-event days (Fig. 4c-d), when the aerosol size distribution was undisturbed by newly formed ultrafine particles and the corresponding VF_{Acc.} maintained around a high level of 0.95 (Fig. 4a-b). The notably positive correlation between *f*(RH) and R_{eff} could be linked to the secondary formation of hygroscopic particles within the accumulation mode, primarily via photochemical reactions and further intensified by heatwaves during the non-event day particularly of the P2 period (Gu et al., 2023; Liu et al., 2014; R. Zhang et al., 2015; Zhang et al., 2024). Consequently, *f*(RH) at a specific R_{eff} was generally higher during the P2 period in comparison to that of P1 (Fig. 4c-d), also with high *f*(RH) levels observed for smaller size cases of R_{eff} <110 nm under some extremely high temperature conditions (T >40 °C, as highlighted by the red dashed circle in Fig. 4d). The higher SOC/OC on P2 non-event days further demonstrated the stronger secondary aerosol formation in comparison to P1 non-event days (Fig. S3b).

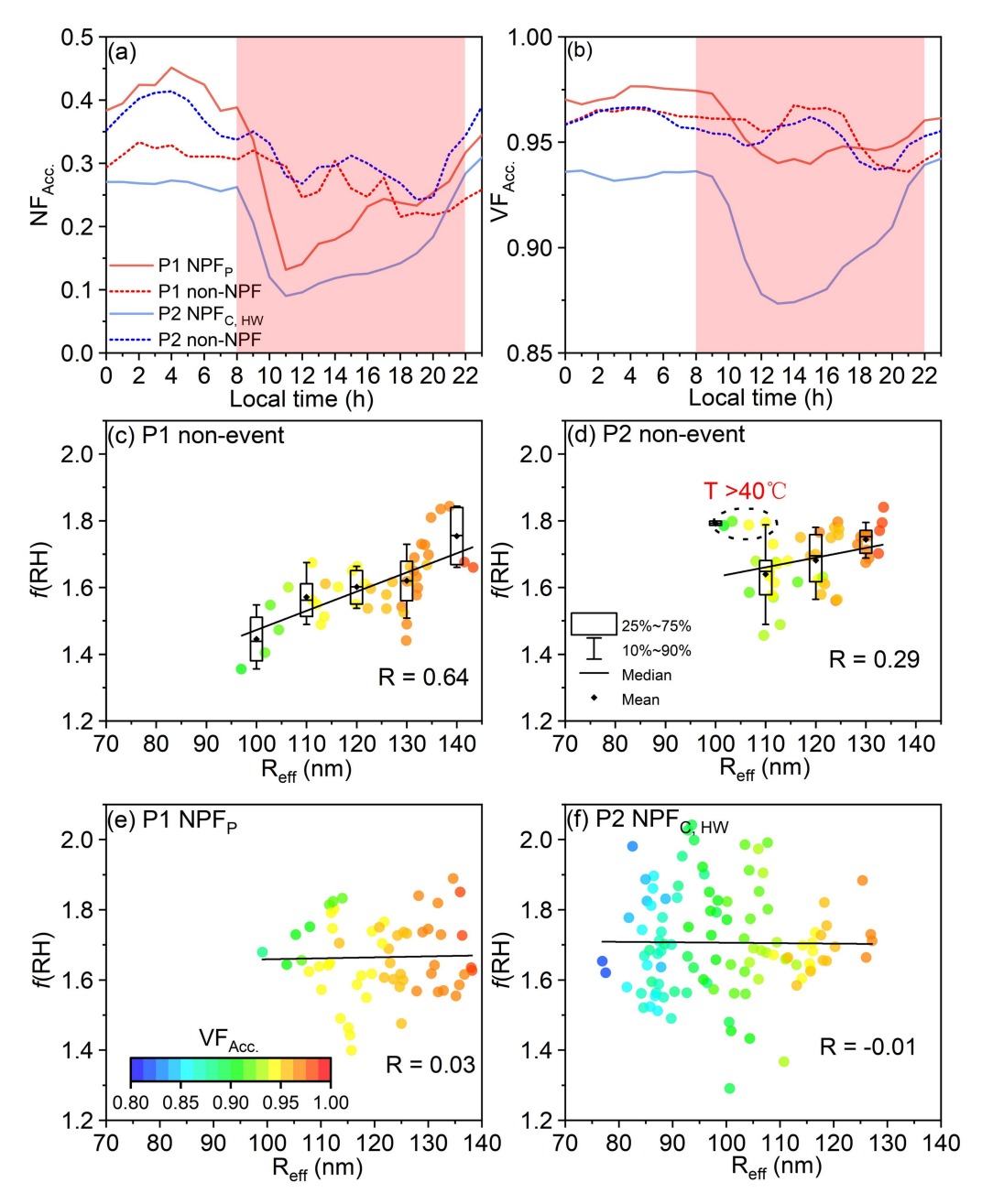


Figure 4. Diurnal variations of **(a)** the number fraction (NF_{Acc.}) and **(b)** volume fraction of accumulation mode particles (VF_{Acc.}) on P1 (red) and P2 (blue) NPF days (solid line), as well as non-event days (dash line). The time window of 08:00-22:00 LT was shaded in red. The relationship of *f*(RH) with R_{eff} and VF_{Acc.} (as indicated by the colored dots) on P1 **(c)** and P2 non-event days **(d)**, as well as on P1 **(e)** and P2 **(f)** NPF days during the 08:00-22:00 LT time window.

Nevertheless, f(RH) was almost independent of the two parameters (i.e., R_{eff} and VF_{Acc.}) for NPF events (Fig. 4e-f). This is mainly due to the explosive formation of ultrafine particles and subsequent growth on NPF days, significantly altering

aerosol size distributions and inducing large fluctuations in the number and volume fractions of accumulation mode particles (as shaded in Fig. 4a-b). Therefore, characterizing f(RH) with the corresponding R_{eff} of aerosol populations was no longer applicable. Alternatively, SAE was commonly used to estimate or parameterize f(RH) (Titos et al., 2014; Xia et al., 2023; Xue et al., 2022), in line with the similar diurnal patterns of f(RH) and SAE observed in this study. Figure 5 demonstrated a significantly positive correlation between f(RH) and SAE during NPF days in comparison to non-event days, with a similar slope of approximately 0.65 suggesting the consistent variation of f(RH) with SAE across both periods. As larger particles contributed higher to the aerosol volume concentrations (Fig. S5), the decrease of SAE also corresponded to an increase in $\sigma_{sca, 525}$ (Fig. 5a3, b3). Given that larger $\sigma_{\text{sca}, 525}$ values typically indicate the condition of a higher aerosol loading, f(RH)increased with SAE whereas decreased with $\sigma_{sca, 525}$, or rather the pollution level, during NPF days. The cleaner environment of P2 period generally possessed a lower CS (Table S2, as denoted by the size of circles in Fig. 5a2, b2), thereby in favor of the occurrence of NPF event. Aerosol f(RH) and SAE exhibited a higher level on P2 NPF_{C, HW} days (as shown by the dash lines in Fig. 5), the possible reasons can be attributed to the following two aspects. One is related to the smaller aerosol Reff (with a larger SAE) due to the lower FR and GR, likely influenced by the evaporation of newly-formed unstable clusters and particle coatings under heatwaves (Bousiotis et al., 2021; Cusack et al., 2013; Deng et al., 2020) during the subsequent growth of aerosols. Secondly, the higher temperature was normally associated with stronger photochemical oxidation, which could intensify the formation of secondary aerosol components with a higher hygroscopicity (Asmi et al., 2010; Gu et al., 2023; Liu et al., 2014; Wu et al., 2016; R. Zhang et al., 2015; Zhang et al., 2024). This is further supported by the slightly higher levels of UVB (P1: $2.6 \pm 1.9 \text{ W} \cdot \text{m}^{-2}$ versus P2: $2.7 \pm 1.9 \text{ W} \cdot \text{m}^{-2}$ 2.0 W·m⁻²) and O₃/O_X (P1: 0.81 \pm 0.17 versus P2: 0.82 \pm 0.17) during P2 heatwave days, also in line with a recent study which demonstrated that heatwaves affected secondary organic aerosols (SOA) formation and aging by accelerating photooxidation in Beijing (Zhang et al., 2024).

483

484

485

486

487

488

489

490

491

492

493

494

495

496

497

498

499

500

501

502

503

504

505

506

507

508

509

510

511

It is worth noting that f(RH) did not show a consistently higher level after the NPF_{C, HW} occurrence during P2 period, and it was slightly higher within the first few hours of NPF occurrence (i.e., ~ 12:00 -15:00 LT) on P1 NPF_P days (Fig. 3b). In fact, aerosol optical hygroscopicity not fully corresponds to the bulk hygroscopicity primarily determined by aerosol chemical components, and the variability in aerosol optical features also plays a key role in f(RH). Hence, the size-dependency of aerosol optical properties should be considered. The size-resolved $\sigma_{sca, 525}$ distribution and size-resolved cumulative frequency distribution (CFD) of $\sigma_{sca, 525}$ over different NPF days were calculated using the Mie theory, with good agreements between the theoretically calculated and measured $\sigma_{sca, 525}$ values (R² = 0.99). As shown in Fig. S10a and Fig. S12, new particles must grow into the accumulation mode size at least before they can exert a significant influence on the total scattering coefficient. The critical sizes corresponding to the cumulative frequency of 50% in $\sigma_{sca, 525}$ were 358.7 nm and 333.8 nm on P1 and P2 NPF days, respectively. This indicates that relatively smaller particles including the newly formed and grown ones mixed with pre-existing and aged particles contributed a slightly higher portion to σ_{sca, 525} on P2 NPF_{C, HW} days, while the $\sigma_{sca, 525}$ was mainly contributed by larger ones on P1 NPF_P days. Nevertheless, the Mie theory suggests that these smaller particles generally have a weaker enhancement in total scattering after hygroscopic growth, in comparison to larger size particles (Collaud Coen et al., 2007, Fig. S10a). Consequently, the changes in aerosol optical and hygroscopic properties necessitate consideration of both aerosol optical and chemical characteristics during different NPF events. Newly formed ultrafine particles contributed minor to aerosol optical properties, resulting in a lower f(RH) during the initial hours of P2 NPF_{C, HW} events compared to that of P1 NPF_P events (Fig. 3b), as evidenced by a smaller R_{eff} for P2 NPF_{C, HW} events (Fig. S6). In contrast, the growth of pre-existing and newly formed particles into larger sizes would subsequently affect bulk aerosol optical properties, which was evidenced by the enhancement in aerosol extinction coefficient observed after NPF occurrence in a recent study (Sun et al., 2024). Specifically, particles could undergo a longer and more intensified photochemical aging process during NPF_C, HW events as influenced by

513

514

515

516

517

518

519

520

521

522

523

524

525

526

527

528

529

530

531

532

533

534

535

536

537

538

539

540

541

persistent heatwaves, which facilitated the secondary formation of hygroscopic aerosols and resulted in a higher *f*(RH) after 15:00 LT (Fig. 3b).

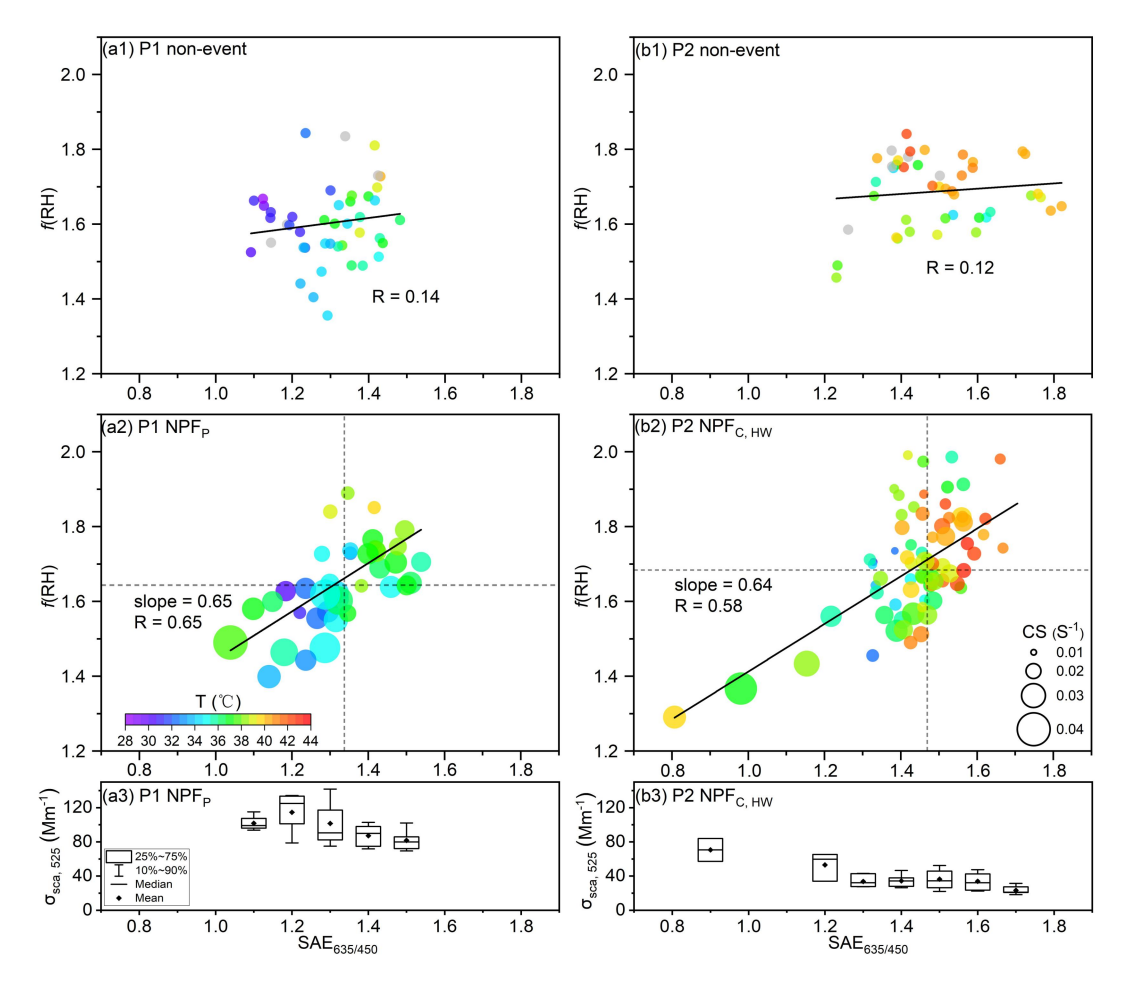


Figure 5. The relationship between f(RH) and $SAE_{635/450}$, as well as temperature (as indicated by the color of dots, missing values are represented in gray) and CS (as denoted by the size of circles), on P1 non-event days **(a1)**, NPF_P days **(a2)** during the 08:00-22:00 LT time window. The vertical (horizontal) dash line represents the median value of $SAE_{635/450}$ (f(RH)). **(a3)** The corresponding σ_{sca} , 525 under different $SAE_{635/450}$ levels on P1 NPF_P days. **(b1-b3)** The same but for P2 period.

3.5 f(RH)-induced changes in aerosol direct radiative forcing

The changes in f(RH) have significant implications for aerosol direct radiative forcing. Despite considerably lower $\sigma_{sca, 525}$ results during heatwaves, the corresponding mean $f_{RF}(RH)$ levels particularly for P2 NPF_{C, HW} days were higher than that of the P1 cases (Fig. 6a). A robust positive correlation (R² = 0.68) was observed between f(RH) and aerosol radiative forcing enhancement factor, $f_{RF}(RH)$

(Fig. 6b). This is likely attributed to the enhanced $f_{RF}(RH)$ with the larger forward scattering ratio β , or rather higher HBF for smaller particle sizes, as supported by a generally negative correlation between $f_{RF}(RH)$ and R_{eff} . Specifically, the highest $f_{RF}(RH)$ value of 2.21 \pm 0.23 was observed on P2 NPF_{C, HW} days, characterized with the highest f(RH) and smallest R_{eff} (i.e., highest HBF) of the entire study period.

558

559

560

561

562

563

564

565

566

567

568

569

570

571

572

573

574

575

576

577

578

579

580

581

582

583

584

585

586

587

The definition of $f_{RF}(RH)$ in Eq.(5) implies the dependences of $f_{RF}(RH)$ on both f(RH) and HBF-derived $\beta(RH)$ and $\beta(dry)$, or rather the ratio of HBF_{525. RH}/HBF₅₂₅. The mean HBF_{525, RH} was generally larger than HBF₅₂₅ in this study, specifically with the HBF_{525, RH}/HBF₅₂₅ ratios centered around 1.8 and even approached 2.5 on P2 NPF_{C, HW} days (Fig. 6c, Table S2). This could be different from the classical Mie theory with the spherical-particle premise, i.e., the observed light backscattering was enhanced after hydration likely resulted from the evolution in particle morphology that significantly influences their optical properties (Mishchenko 2009). The organic-rich particles might remain non-spherical even after water uptake due to the efficient evaporation of organic coatings under extremely hot weather conditions, as evidenced by a recent study that high temperature conditions could accelerate the evaporation rate of SOA (Li et al., 2019). Given that the backward scattering intensity of non-spherical particles is suggested to be much larger than its spherical counterparts at scattering angles between 90° and 150° (Mishchenko 2009; Yang et al., 2007) and that the HBF-derived asymmetry parameter (g) normally correlates positively with the aerosol forward scattering (Andrews et al., 2006; Marshall et al., 1995), the generally smaller g_{RH} results (in comparison to g) confirmed the decrease (increase) in the forward (backward) light scattering after water uptake (Fig. S10b), likely implying the change in the morphological structure of particles. This is particularly evident for P2 NPF_{C, HW} days, with a much lower level of g_{RH} was observed (Fig. S10b). Another possible reason is that although the abundant newly formed particles were generally optically-insensitive, their contributions to $\sigma_{sca, 525}$ and especially to $\sigma_{bsca, 525}$ could be amplified upon humidification. Namely, even if these hydrated particles remained small (e.g., below 100 nm), their HBF was significantly higher than that of larger particles (Fig. S10a), thereby elevating the corresponding

HBF_{525, RH} levels during NPF events. These combined effects could potentially change particle morphology and optical properties (e.g., elevated the HBF_{525, RH}) particularly during heatwave-influenced NPF_{C, HW} days, characterized with the smallest aerosol $R_{\rm eff}$ (102.8 ± 12.4 nm) (Figure. S6), lowest number fraction of accumulation mode particles (0.20 ± 0.10), and a higher SOC/OC ratio. The higher HBF_{525, RH}/HBF₅₂₅ ratios increased the HBF-derived β(RH)/β(dry) levels, in combination of the elevated f(RH), further resulting in the highest $f_{RF}(RH)$ observed during P2 NPF_{C, HW} events. Given that previously observed HBF_{525, RH} was typically lower than HBF₅₂₅ (Titos et al., 2021; Xia et al., 2023; L. Zhang et al., 2015), the mean $f_{RF}(RH)$ results of this study ($f_{RF}(85\%) = 2.05 \pm 0.24$) were significantly higher than those observed in the Yangtze River Delta ($f_{RF}(85\%) = 1.5$, L. Zhang et al., 2015), the North China Plain ($f_{RF}(80\%) = 1.6 \pm 0.2$, Xia et al., 2023), and some other regions in the world (Titos et al., 2021, Fig. 6d). It should be noted that the reported $f_{RF}(RH)$ for the UGR site (Spain) was even higher, likely due to the higher R_s and α_s used in the derivation of $f_{RF}(RH)$ in that area (Titos et al., 2021).

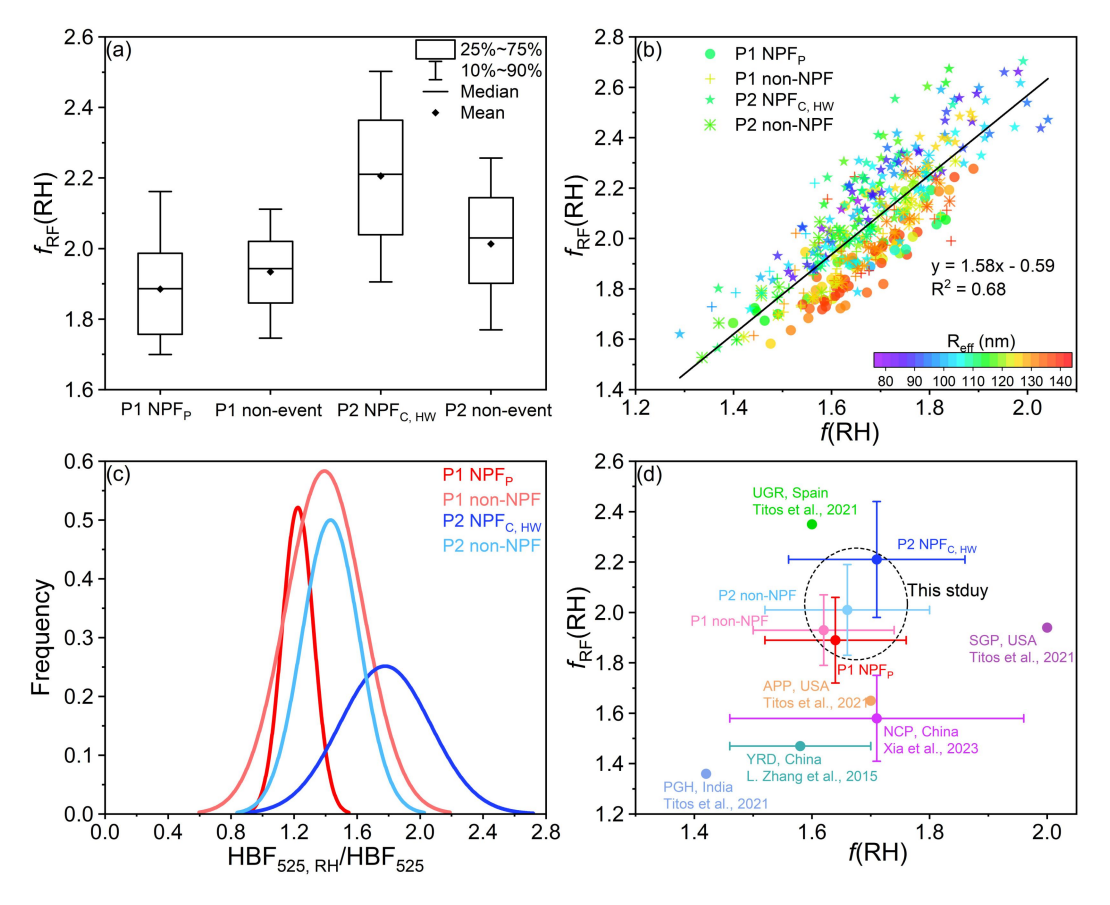


Figure 6. (a) The box-plot of $f_{RF}(RH)$ during P1 or P2 NPF event and non-event days. (b) The relationship between $f_{RF}(RH)$ and f(RH), as colored by the corresponding R_{eff} , during P1 or P2 NPF and non-event days (shown in different symbols). (c) Occurrence frequency of the HBF₅₂₅, $_{RH}/HBF_{525}$ ratios during P1 or P2 NPF and non-event days. (d) The mean $f_{RF}(RH)$ under different f(RH) levels (the error bars stand for \pm one standard deviations corresponding to $f_{RF}(RH)$ and f(RH), respectively), along with the reported $f_{RF}(RH)$ and f(RH) data for other regions in the world.

611

612

613

614

615

616

617

618

619

620

621

622

623

624

625

626

627

628

629

630

631

632

633

A recent study has indicated that continuous reduction of PM_{2.5} mass loadings can increase the net solar radiation, thereby promoting NPF events (Zhao et al., 2021). Given the complexity and dynamic evolution of the atmospheric environment, these can further alter the intrinsic properties of aerosol particles (e.g., f(RH), HBF, morphology), potentially feeding back into aerosol-radiation interactions. Our findings suggest that NPF and growth events may elevate aerosol optical hygroscopicity in rather hot environments, e.g., the Basin area and tropical regions. Meanwhile, NPF serves as a crucial secondary transformation process in the atmosphere (Zhu et al., 2021). The favorable atmospheric diffusion capability ensured the mixing of newly formed particles into the upper boundary layer, where is colder and more humid than that near the surface during heatwaves (Jin et al., 2022). Hence, the enhancement of aerosol optical hygroscopicity during the subsequent growth of pre-existing and newly formed particles possibly exacerbates secondary pollution and even triggers haze events (Hao et al., 2024; Kulmala et al., 2021). On the other hand, a large number of studies have demonstrated that the new particles of higher hygroscopicity could contribute more to the activation of CCN (Ma et al., 2016; Ren et al., 2021; Rosati et al., 2022; Sun et al., 2024; Wu et al., 2015), thereby modulating the aerosol-cloud interactions and further the global climate (Fan et al., 2016; Merikanto et al., 2006; Westervelt et al., 2013). Additionally, the simultaneous decrease in aerosol effective radius and possibly evaporation-induced non-spherical particle morphology further enhance the aerosol direct radiative forcing enhancement factor, potentially amplifying the cooling effect mainly caused by light scattering aerosols. This highlights the needs for further in-depth exploration on aerosol

radiative impacts at weather extremes (e.g., heatwaves) with the changing climate, given the continuous reductions of anthropogenic emissions and more intense emissions of biogenic origins with the global warming. Besides, more detailed information on the evolution of particle morphology with the changing environment (e.g., varied temperature and RH) would enrich insights into the aerosol radiative forcing.

4 Conclusions and implications

A rare heatwave event raged throughout urban Chongqing of southwest China in the summer of 2022, which significantly influenced aerosol physicochemical properties and atmospheric processes (e.g., NPF and subsequent growth). Concurrent measurements of aerosol optical and hygroscopic properties, PNSD, and bulk chemical compositions were conducted to explore the mechanisms behind the variations in aerosol optical hygroscopicity during different NPF days under diverse weather conditions.

NPF events exhibited distinct characteristics during the normally hot (P1, relatively polluted) and heatwaves-dominated (P2, quite clean) periods. NPF_P within P1 period was favored by the decrease in background aerosol loading and the higher abundance of H₂SO₄. NPF_{C, HW} events that occurred during the heatwave P2 period were characterized with lower CS, CoagS, FR and GR, as well as smaller R_{eff} and D_{mode}, than P1 NPF_P cases. In comparison to the P1 NPF_P events, NPF_{C, HW} occurred approximately one hour earlier and the subsequent growth was longer during P2, likely intensifying the photochemical oxidation due to heatwave-influenced aging processes and modulating the evolution of aerosol size distributions differently. Furthermore, significant differences in aerosol optical and hygroscopic properties were observed between the normally hot and heatwave-dominated NPF days. The newly formed and grown particles mixed with pre-existing aerosols contributed a minor σ_{sca, 525} noontime peak occurred on the much cleaner P2 NPF_{C, HW} days, while

the $\sigma_{sca, 525}$ peaked earlier around the morning rush hours on P1 NPF_P days. HBF and SAE were significantly higher on P2 NPF_{C, HW} days, primarily due to the smaller R_{eff} for heatwave-influenced NPF_{C, HW} cases. f(RH) remained relatively stable during the daytime of NPF days and peaked around 16:00-18:00 LT. Specifically, aerosol optical hygroscopicity tended to be higher during the subsequent growth and aging of both pre-existing particles and newly formed ones on P2 NPF_{C, HW} days than that for P1 NPF_P days, which aligned with the higher f_W levels.

Compared with non-event cases, the generally higher levels of daily mean f(RH) suggested that the aerosol optical hygroscopicity was enhanced on NPF days in hot summer of urban Chongqing. A significantly positive (negative) correlation between f(RH) and SAE (CS, $\sigma_{sca, 525}$, or rather the pollution level) was observed on NPF days for both periods, accompanied by higher f(RH) and SAE values on NPF_{C, HW} days. This was likely due to the evaporation of both unstable clusters and particle coatings under heatwaves (Bousiotis et al., 2021; Cusack et al., 2013; Deng et al., 2020; Garmash et al., 2024), thereby reducing aerosol sizes (e.g., Reff, Dmode) whereas increasing SAE. Moreover, heatwave-influenced stronger photooxidation enhanced the formation of more hygroscopic secondary components during the subsequent growth/aging processes of both pre-existing and newly formed particles on P2 NPF_{C, HW} days in comparison to that of P1 NPF_P cases. The aerosol light scattering or volume concentration was mainly contributed by the larger accumulation-mode particles, while more ultrafine particles dominated the size distribution especially for the initial stage of heatwave-influenced NPF_{C, HW} events, further leading to a lower f(RH) following the NPF occurrence (i.e., ~ 12:00 -15:00 LT) in comparison to P1 NPF_P days.

Changes in f(RH) could potentially impact the aerosol direct radiative forcing. A robust positive (negative) correlation existed between $f_{RF}(RH)$ and f(RH) (R_{eff}). Despite a lower σ_{sca} , 525 during heatwaves, the corresponding mean $f_{RF}(RH)$ was relatively higher and the maximum value of 2.21 ± 0.23 was observed on P2 NPF_{C, HW} days, associated with the highest f(RH) (1.71 ± 0.13), smallest R_{eff} (102.8 ± 12.4 nm), and highest HBF_{525, RH}/HBF₅₂₅ ratios (1.78 ± 0.29). The above highlights that

heatwaves could influence the NPF and atmospheric processing (although with a decreased aerosol $R_{\rm eff}$ and $D_{\rm mode}$ likely due to evaporation-resulted non-spherical particle morphology under persistently high temperature conditions), thereby enhancing aerosol optical hygroscopic growth and potentially reducing the net solar radiation directly especially in hot summer. Further explorations on detailed molecular-scale characterizations (e.g., molecular structures and compositions of newly and secondary formed particles, as well as particle morphology) and aerosol radiative impacts including the aerosol-cloud interactions of weather extremes (e.g., heatwaves) with the changing climate are highly recommended.

Data availability. Data will be available upon request.

Author contributions. YH and PL: Methodology, Investigation, Data analysis,
Formal analysis, Visualization, Validation, Writing – original draft & editing. YG and
ZW: Methodology, Investigation, Formal analysis. MT, YC, HX and WH: Data
curation, Methodology. FW and YL: Investigation. YK: Methodology, Data analysis,
Writing – review & editing. JC: Conceptualization, Methodology, Funding acquisition,
Data curation, Writing – review & editing, Supervision.

Competing interests. The authors declare no competing financial interest.

Acknowledgement. This work was supported by the National Natural Science Foundation of China (No. 42105075), Venture and Innovation Support Program for Chongqing Overseas Returnees (No. cx2021021). We thank Biao Xue for the technical support on the utilization and maintenance of the humidified nephelometer system. We also thank Ziqian Wang for the TSP filter sample collection and Jiawei Zhou for the corresponding offline chemical analysis.

720 References

- 721 An, J., Lu, Y., Huang, D. D., Ding, X., Hu, Q., Yan, R., Qiao, L., Zhou, M., Huang, C.,
- Wang, H., Fu, Q., Yu, F., and Wang, L.: Sectoral Size Resolved Particle Number
- 723 Emissions With Speciation: Emission Profile Based Quantification and a Case Study
- 724 in the Yangtze River Delta Region, China, J. Geophys. Res. Atmos., 1–22,
- 725 https://doi.org/10.1029/2024JD041234, 2024.
- Andrews, E., Sheridan, P. J., Fiebig, M., McComiskey, A., Ogren, J. A., Arnott, P.,
- 727 Covert, D., Elleman, R., Gasparini, R., Collins, D., Jonsson, H., Schmid, B., and
- Wang, J.: Comparison of methods for deriving aerosol asymmetry parameter, J.
- 729 Geophys. Res. Atmos., 111, 1–16, https://doi.org/10.1029/2004JD005734, 2006.
- 730 Asmi, E., Frey, A., Virkkula, A., Ehn, M., Manninen, H. E., Timonen, H.,
- 731 Tolonen-Kivimäki, O., Aurela, M., Hillamo, R., and Kulmala, M.: Hygroscopicity and
- chemical composition of antarctic sub-micrometre aerosol particles and observations
- of new particle formation, Atmos. Chem. Phys., 10, 4253–4271,
- 734 https://doi.org/10.5194/acp-10-4253-2010, 2010.
- 735 Bae, M. S., Lee, T., Schauer, J. J., Park, G., Son, Y. B., Kim, K. H., Cho, S. S., Park,
- S. S., Park, K., and Shon, Z. H.: Chemical Characteristics of Size-Resolved Aerosols
- 737 in Coastal Areas during KORUS-AQ Campaign; Comparison of Ion Neutralization
- 738 Model, Asia-Pacific J. Atmos. Sci., 55, 387–399,
- 739 https://doi.org/10.1007/s13143-018-00099-1, 2019.
- Bousiotis, D., Brean, J., Pope, F. D., Dall'Osto, M., Querol, X., Alastuey, A., Perez,
- N., Petäjä, T., Massling, A., Klenø Nøjgaard, J., Nordstrøm, C., Kouvarakis, G.,
- Vratolis, S., Eleftheriadis, K., Niemi, J. V., Portin, H., Wiedensohler, A., Weinhold,
- 743 K., Merkel, M., Tuch, T., and Harrison, R. M.: The effect of meteorological
- 744 conditions and atmospheric composition in the occurrence and development of new
- particle formation (NPF) events in Europe, Atmos. Chem. Phys., 21, 3345–3370,
- 746 https://doi.org/10.5194/acp-21-3345-2021, 2021.

- Prooke Anderson, G. and Bell, M. L.: Heat waves in the United States: Mortality risk
- during heat waves and effect modification by heat wave characteristics in 43 U.S.
- 749 communities, Environ. Health Perspect., 119, 210–218,
- 750 https://doi.org/10.1289/ehp.1002313, 2011.
- 751 Chen, J., Zhao, C. S., Ma, N., and Yan, P.: Aerosol hygroscopicity parameter derived
- 752 from the light scattering enhancement factor measurements in the North China Plain,
- 753 Atmos. Chem. Phys., 14, 8105–8118, https://doi.org/10.5194/acp-14-8105-2014,
- 754 2014.
- 755 Chen, Q., Mu, Z., Song, W., Wang, Y., Yang, Z., Zhang, L., and Zhang, Y. L.:
- 756 Size-Resolved Characterization of the Chromophores in Atmospheric Particulate
- 757 Matter From a Typical Coal-Burning City in China, J. Geophys. Res. Atmos., 124,
- 758 10546–10563, https://doi.org/10.1029/2019JD031149, 2019.
- 759 Chen, T., Wang, T., Xue, L., and Brasseur, G.: Heatwave exacerbates air pollution in
- 760 China through intertwined climate-energy-environment interactions, Sci. Bull., 69,
- 761 2765–2775, https://doi.org/10.1016/j.scib.2024.05.018, 2024.
- 762 China Meteorological Administration, 2022. China Climate Bulletin 2022.
- 763 https://www.cma.gov.cn/zfxxgk/gknr/qxbg/202303/t20230324 5396394.html.
- Accessed on 23 March 2023. (in Chinese).
- Cho Cheung, H., Chung-Kuang Chou, C., Siu Lan Lee, C., Kuo, W. C., and Chang, S.
- 766 C.: Hygroscopic properties and cloud condensation nuclei activity of atmospheric
- aerosols under the influences of Asian continental outflow and new particle formation
- at a coastal site in eastern Asia, Atmos. Chem. Phys., 20, 5911-5922,
- 769 https://doi.org/10.5194/acp-20-5911-2020, 2020.
- 770 Chylek, P. and Wong, J.: Effect of absorbing aerosols on global radiation budget,
- 771 Geophys. Res. Lett., 22, 929–931, https://doi.org/10.1029/95GL00800, 1995.

- Collaud Coen, M., Weingartner, E., Nyeki, S., Cozic, J., Henning, S., Verheggen, B.,
- Gehrig, R., and Baltensperger, U.: Long-term trend analysis of aerosol variables at the
- 774 high-alpine site Jungfraujoch, J. Geophys. Res. Atmos., 112,
- 775 https://doi.org/10.1029/2006JD007995, 2007.
- Covert, D. S., Charlson, R. J., and Ahlquist, N. C.: A Study of the Relationship of
- 777 Chemical Composition and Humidity to Light Scattering by Aerosols, J. Appl.
- 778 Meteorol., 11, 968–976,
- 779 https://doi.org/10.1175/1520-0450(1972)011<0968:asotro>2.0.co;2, 1972.
- 780 Crumeyrolle, S., Kontkanen, J. S. S., Rose, C., Velazquez Garcia, A., Bourrianne, E.,
- Catalfamo, M., Riffault, V., Tison, E., Ferreira De Brito, J., Visez, N., Ferlay, N.,
- 782 Auriol, F., and Chiapello, I.: Measurement report: Atmospheric new particle
- formation at a peri-urban site in Lille, northern France, Atmos. Chem. Phys., 23,
- 784 183–201, https://doi.org/10.5194/acp-23-183-2023, 2023.
- Cusack, M., Alastuey, A., and Querol, X.: Case studies of new particle formation and
- 786 evaporation processes in the western Mediterranean regional background, Atmos.
- 787 Environ., 81, 651–659, https://doi.org/10.1016/j.atmosenv.2013.09.025, 2013.
- Dada, L., Paasonen, P., Nieminen, T., Buenrostro Mazon, S., Kontkanen, J., Peräkylä,
- O., Lehtipalo, K., Hussein, T., Petäjä, T., Kerminen, V. M., Bäck, J., and Kulmala, M.:
- 790 Long-term analysis of clear-sky new particle formation events and nonevents in
- 791 Hyytiälä, Atmos. Chem. Phys., 17, 6227–6241,
- 792 https://doi.org/10.5194/acp-17-6227-2017, 2017.
- Dal Maso, M., Kulmala, M., Riipinen, I., Wagner, R., Hussein, T., Aalto, P. P., and
- Lehtinen, K. E. J.: Formation and growth of fresh atmospheric aerosols: Eight years
- of aerosol size distribution data from SMEAR II, Hyytiälä, Finland, Boreal Environ.
- 796 Res., 10, 323–336, 2005.

- Delene, D. J. and Ogren, J. A.: Variability of aerosol optical properties at four North
- 798 American surface monitoring sites, J. Atmos. Sci., 59, 1135–1150,
- 799 https://doi.org/10.1175/1520-0469(2002)059<1135:VOAOPA>2.0.CO;2, 2002.
- Deng, C., Cai, R., Yan, C., Zheng, J., and Jiang, J.: Formation and growth of sub-3
- nm particles in megacities: Impact of background aerosols, Faraday Discuss., 226,
- 802 348–363, https://doi.org/10.1039/d0fd00083c, 2021.
- 803 Deng, C., Fu, Y., Dada, L., Yan, C., Cai, R., Yang, D., Zhou, Y., Yin, R., Lu, Y., Li,
- X., Qiao, X., Fan, X., Nie, W., Kontkanen, J., Kangasluoma, J., Chu, B., Ding, A.,
- Kerminen, V. M., Paasonen, P., Worsnop, D. R., Bianchi, F., Liu, Y., Zheng, J., Wang,
- 806 L., Kulmala, M., and Jiang, J.: Seasonal characteristics of new particle formation and
- 807 growth in urban Beijing, Environ. Sci. Technol., 54, 8547–8557,
- 808 https://doi.org/10.1021/acs.est.0c00808, 2020.
- 809 Duan, J., Huang, R. J., Wang, Y., Xu, W., Zhong, H., Lin, C., Huang, W., Gu, Y.,
- 810 Ovadnevaite, J., Ceburnis, D., and O'Dowd, C.: Measurement report: Size-resolved
- secondary organic aerosol formation modulated by aerosol water uptake in wintertime
- haze, Atmos. Chem. Phys., 24, 7687–7698, https://doi.org/10.5194/acp-24-7687-2024,
- 813 2024.
- Fan, J., Wang, Y., Rosenfeld, D., and Liu, X.: Review of aerosol-cloud interactions:
- Mechanisms, significance, and challenges, J. Atmos. Sci., 73, 4221–4252,
- 816 https://doi.org/10.1175/JAS-D-16-0037.1, 2016.
- Fierz-Schmidhauser, R., Zieger, P., Gysel, M., Kammermann, L., Decarlo, P. F.,
- 818 Baltensperger, U., and Weingartner, E.: Measured and predicted aerosol light
- scattering enhancement factors at the high alpine site Jungfraujoch, Atmos. Chem.
- 820 Phys, 10, 2319–2333, 2010.
- 621 Garmash, O., Ezhova, E., Arshinov, M., Belan, B., Lampilahti, A., Davydov, D., Räty,
- M., Aliaga, D., Baalbaki, R., Chan, T., Bianchi, F., Kerminen, V. M., Petäjä, T., and

- 823 Kulmala, M.: Heatwave reveals potential for enhanced aerosol formation in Siberian
- 824 boreal forest, Environ. Res. Lett., 19, https://doi.org/10.1088/1748-9326/ad10d5,
- 825 2024.
- 826 Gu, Y., Huang, R. J., Duan, J., Xu, W., Lin, C., Zhong, H., Wang, Y., Ni, H., Liu, Q.,
- 827 Xu, R., Wang, L., and Li, Y. J.: Multiple pathways for the formation of secondary
- organic aerosol in the North China Plain in summer, Atmos. Chem. Phys., 23,
- 5419–5433, https://doi.org/10.5194/acp-23-5419-2023, 2023.
- Guenther, A. B., Monson, R. K., and Fall, R.: Isoprene and monoterpene emission
- 831 rate variability: Observations with eucalyptus and emission rate algorithm
- development, J. Geophys. Res. Atmos., 96, 10799–10808,
- 833 https://doi.org/10.1029/91jd00960, 1991.
- 834 Guo, X., Huang, J., Luo, Y., Zhao, Z., and Xu, Y.: Projection of heat waves over
- 835 China for eight different global warming targets using 12 CMIP5 models, Theor. Appl.
- 836 Climatol., 128, 507–522, https://doi.org/10.1007/s00704-015-1718-1, 2016.
- Hamed, A., Joutsensaari, J., Mikkonen, S., Sogacheva, L., Dal Maso, M., Kulmala,
- 838 M., Cavalli, F., Fuzzi, S., Facchini, M. C., Decesari, S., Mircea, M., Lehtinen, K. E. J.,
- and Laaksonen, A.: Nucleation and growth of new particles in Po Valley, Italy, Atmos.
- 840 Chem. Phys., 7, 355–376, https://doi.org/10.5194/acp-7-355-2007, 2007.
- Hamed, A., Korhonen, H., Sihto, S. L., Joutsensaari, J., Jrvinen, H., Petäjä, T., Arnold,
- 842 F., Nieminen, T., Kulmala, M., Smith, J. N., Lehtinen, K. E. J., and Laaksonen, A.:
- The role of relative humidity in continental new particle formation, J. Geophys. Res.
- 844 Atmos., 116, 1–12, https://doi.org/10.1029/2010JD014186, 2011.
- Hand, J. L. and Malm, W. C.: Review of aerosol mass scattering efficiencies from
- ground-based measurements since 1990, J. Geophys. Res. Atmos., 112,
- 847 https://doi.org/10.1029/2007JD008484, 2007.

- Hao, Y., Gou, Y., Wang, Z., Huang, W., Wan, F., Tian, M., and Chen, J.: Current
- challenges in the visibility improvement of urban Chongqing in Southwest China:
- From the perspective of PM2.5-bound water uptake property over 2015–2021, Atmos.
- 851 Res., 300, 107215, https://doi.org/10.1016/j.atmosres.2023.107215, 2024.
- 852 Hao, Z., Chen, Y., Feng, S., Liao, Z., An, N., and Li, P.: The 2022
- 853 Sichuan-Chongqing spatio-temporally compound extremes: a bitter taste of novel
- hazards, Sci. Bull., 68, 1337–1339, https://doi.org/10.1016/j.scib.2023.05.034, 2023.
- Hauser, M., Orth, R., and Seneviratne, S. I.: Role of soil moisture versus recent
- climate change for the 2010 heat wave in western Russia, Geophys. Res. Lett., 43,
- 857 2819–2826, https://doi.org/10.1002/2016GL068036, 2016.
- Jefferson, A., Hageman, D., Morrow, H., Mei, F., and Watson, T.: Seven years of
- aerosol scattering hygroscopic growth measurements from SGP: Factors influencing
- 860 water uptake, J. Geophys. Res. Atmos., 122, 9451–9466,
- 861 https://doi.org/10.1002/2017JD026804, 2017.
- 862 Jin, X., Li, Z., Wu, T., Wang, Y., Cheng, Y., Su, T., Wei, J., Ren, R., Wu, H., Li, S.,
- 263 Zhang, D., and Cribb, M.: The different sensitivities of aerosol optical properties to
- particle concentration, humidity, and hygroscopicity between the surface level and the
- upper boundary layer in Guangzhou, China, Sci. Total Environ., 803, 150010,
- 866 https://doi.org/10.1016/j.scitotenv.2021.150010, 2022.
- Kerminen, V. M., Chen, X., Vakkari, V., Petäjä, T., Kulmala, M., and Bianchi, F.:
- 868 Atmospheric new particle formation and growth: Review of field observations,
- 869 Environ. Res. Lett., 13, https://doi.org/10.1088/1748-9326/aadf3c, 2018.
- Kim, N., Yum, S. S., Park, M., Park, J. S., Shin, H. J., and Ahn, J. Y.: Hygroscopicity
- of urban aerosols and its link to size-resolved chemical composition during spring and
- 872 summer in Seoul, Korea, Atmos. Chem. Phys., 20, 11245–11262,
- 873 https://doi.org/10.5194/acp-20-11245-2020, 2020.

- Kotchenruther, R. A., Hobbs, P. V., and Hegg, D. A.: Humidification factors for
- atmospheric aerosols off the mid-Atlantic coast of the United States, J. Geophys. Res.
- 876 Atmos., 104, 2239–2251, https://doi.org/10.1029/98JD01751, 1999.
- 877 Kuang, Y., He, Y., Xu, W., Zhao, P., Cheng, Y., Zhao, G., Tao, J., Ma, N., Su, H.,
- Zhang, Y., Sun, J., Cheng, P., Yang, W., Zhang, S., Wu, C., Sun, Y., and Zhao, C.:
- Distinct diurnal variation in organic aerosol hygroscopicity and its relationship with
- 880 oxygenated organic aerosol, Atmos. Chem. Phys., 20, 865-880,
- 881 https://doi.org/10.5194/acp-20-865-2020, 2020.
- 882 Kuang, Y., Zhao, C. S., Zhao, G., Tao, J. C., Xu, W., Ma, N., and Bian, Y. X.: A
- 883 novel method for calculating ambient aerosol liquid water content based on
- measurements of a humidified nephelometer system, Atmos. Meas. Tech., 11,
- 885 2967–2982, https://doi.org/10.5194/amt-11-2967-2018, 2018.
- Kuang, Y., Zhao, C., Tao, J., Bian, Y., Ma, N., and Zhao, G.: A novel method for
- deriving the aerosol hygroscopicity parameter based only on measurements from a
- humidified nephelometer system, Atmos. Chem. Phys., 17, 6651-6662,
- https://doi.org/10.5194/acp-17-6651-2017, 2017.
- Kulmala, M., Dada, L., Daellenbach, K. R., Yan, C., Stolzenburg, D., Kontkanen, J.,
- 891 Ezhova, E., Hakala, S., Tuovinen, S., Kokkonen, T. V., Kurppa, M., Cai, R., Zhou, Y.,
- Yin, R., Baalbaki, R., Chan, T., Chu, B., Deng, C., Fu, Y., Ge, M., He, H., Heikkinen,
- L., Junninen, H., Liu, Y., Lu, Y., Nie, W., Rusanen, A., Vakkari, V., Wang, Y., Yang, G.,
- Yao, L., Zheng, J., Kujansuu, J., Kangasluoma, J., Petaja, T., Paasonen, P., Jarvi, L.,
- Worsnop, D., Ding, A., Liu, Y., Wang, L., Jiang, J., Bianchi, F., and Kerminen, V. M.:
- 896 Is reducing new particle formation a plausible solution to mitigate particulate air
- pollution in Beijing and other Chinese megacities?, Faraday Discuss., 226, 334–347,
- 898 https://doi.org/10.1039/d0fd00078g, 2021.
- Kulmala, M., Petäjä, T., Nieminen, T., Sipilä, M., Manninen, H. E., Lehtipalo, K., Dal
- Maso, M., Aalto, P. P., Junninen, H., Paasonen, P., Riipinen, I., Lehtinen, K. E. J.,

- Laaksonen, A., and Kerminen, V. M.: Measurement of the nucleation of atmospheric
- 902 aerosol particles, Nat. Protoc., 7, 1651–1667, https://doi.org/10.1038/nprot.2012.091,
- 903 2012.
- 804 Kulmala, M.: How Particles Nucleate and Grow, Science, 302, 1000–1001,
- 905 https://doi.org/10.1126/science.1090848, 2003.
- 806 Kurtén, T., Torpo, L., Ding, C. G., Vehkamäki, H., Sundberg, M. R., Laasonen, K.,
- and Kulmala, M.: A density functional study on water-sulfuric acid-ammonia clusters
- and implications for atmospheric cluster formation, J. Geophys. Res. Atmos., 112, 1–7,
- 909 https://doi.org/10.1029/2006JD007391, 2007.
- 910 Li, Y., Ding, Y., and Li, W.: Observed trends in various aspects of compound heat
- 911 waves across China from 1961 to 2015, J. Meteorol. Res., 31, 455–467,
- 912 https://doi.org/10.1007/s13351-017-6150-2, 2017.
- Li, Z., Tikkanen, O. P., Buchholz, A., Hao, L., Kari, E., Yli-Juuti, T., and Virtanen, A.:
- 914 Effect of Decreased Temperature on the Evaporation of α-Pinene Secondary Organic
- 915 Aerosol Particles, ACS Earth Sp. Chem., 3, 2775–2785,
- 916 https://doi.org/10.1021/acsearthspacechem.9b00240, 2019.
- Liu, H. J., Zhao, C. S., Nekat, B., Ma, N., Wiedensohler, A., Van Pinxteren, D.,
- 918 Spindler, G., Müller, K., and Herrmann, H.: Aerosol hygroscopicity derived from
- 919 size-segregated chemical composition and its parameterization in the North China
- 920 Plain, Atmos. Chem. Phys., 14, 2525–2539, https://doi.org/10.5194/acp-14-2525-2014,
- 921 2014.
- 922 Liu, P. F., Zhao, C. S., Göbel, T., Hallbauer, E., Nowak, A., Ran, L., Xu, W. Y., Deng,
- 223 Z. Z., Ma, N., Mildenberger, K., Henning, S., Stratmann, F., and Wiedensohler, A.:
- 924 Hygroscopic properties of aerosol particles at high relative humidity and their diurnal
- variations in the north China plain, Atmos. Chem. Phys., 11, 3479–3494,
- 926 https://doi.org/10.5194/acp-11-3479-2011, 2011.

- 927 Lu, Y., Yan, C., Fu, Y., Chen, Y., Liu, Y., Yang, G., Wang, Y., Bianchi, F., Chu, B.,
- Zhou, Y., Yin, R., Baalbaki, R., Garmash, O., Deng, C., Wang, W., Liu, Y., Petäjä, T.,
- 929 Kerminen, V. M., Jiang, J., Kulmala, M., and Wang, L.: A proxy for atmospheric
- daytime gaseous sulfuric acid concentration in urban Beijing, Atmos. Chem. Phys., 19,
- 931 1971–1983, https://doi.org/10.5194/acp-19-1971-2019, 2019.
- Luoma, K., Virkkula, A., Aalto, P., Petäjä, T., and Kulmala, M.: Over a 10-year record
- of aerosol optical properties at SMEAR II, Atmos. Chem. Phys., 19, 11363-11382,
- 934 https://doi.org/10.5194/acp-19-11363-2019, 2019.
- 935 Ma, C. Sen, Ma, G., and Pincebourde, S.: Survive a Warming Climate: Insect
- Responses to Extreme High Temperatures, Annu. Rev. Entomol., 66, 163-184,
- 937 https://doi.org/10.1146/annurev-ento-041520-074454, 2021.
- 938 Ma, N., Zhao, C., Tao, J., Wu, Z., Kecorius, S., Wang, Z., Groß, J., Liu, H., Bian, Y.,
- 839 Kuang, Y., Teich, M., Spindler, G., Muller, K., Van Pinxteren, D., Herrmann, H., Hu,
- 940 M., and Wiedensohler, A.: Variation of CCN activity during new particle formation
- events in the North China Plain, Atmos. Chem. Phys., 16, 8593-8607,
- 942 https://doi.org/10.5194/acp-16-8593-2016, 2016.
- Marshall, S. F., Covert, D. S., and Charlson, R. J.: Relationship between asymmetry
- 944 parameter and hemispheric backscatter ratio: implications for climate forcing by
- 945 aerosols, Appl. Opt., 34, 5–6, 1995.
- Merikanto, J., Spracklen, D. V, Mann, G. W., Pickering, S. J., and Carslaw, K. S.:
- 947 Atmospheric Chemistry and Physics Impact of nucleation on global CCN, Atmos.
- 948 Chem. Phys, 9, 8601–8616, 2009.
- 949 Mishchenko, M. I.: Electromagnetic scattering by nonspherical particles: A tutorial
- 950 review, J. Quant. Spectrosc. Radiat. Transf., 110, 808-832,
- 951 https://doi.org/10.1016/j.jqsrt.2008.12.005, 2009.

- Nairn, J. R. and Fawcett, R. J. B.: The excess heat factor: A metric for heatwave
- 953 intensity and its use in classifying heatwave severity, Int. J. Environ. Res. Public
- 954 Health, 12, 227–253, https://doi.org/10.3390/ijerph120100227, 2014.
- 955 Petters, M. D. and Kreidenweis, S. M.: A single parameter representation of
- hygroscopic growth and cloud condensation nucleus activity, Atmos. Chem. Phys., 7,
- 957 1961–1971, https://doi.org/10.5194/acp-7-1961-2007, 2007.
- Pierce, T. E. and Waldruff, P. S.: Pc-beis: A personal computer version of the biogenic
- 959 emissions inventory system, J. Air Waste Manag. Assoc., 41, 937-941,
- 960 https://doi.org/10.1080/10473289.1991.10466890, 1991.
- 961 Qi, X. M., Ding, A. J., Nie, W., Petäjä, T., Kerminen, V. M., Herrmann, E., Xie, Y. N.,
- 262 Zheng, L. F., Manninen, H., Aalto, P., Sun, J. N., Xu, Z. N., Chi, X. G., Huang, X.,
- 963 Boy, M., Virkkula, A., Yang, X. Q., Fu, C. B., and Kulmala, M.: Aerosol size
- 964 distribution and new particle formation in the western Yangtze River Delta of China:
- 965 2 years of measurements at the SORPES station, Atmos. Chem. Phys., 15,
- 966 12445–12464, https://doi.org/10.5194/acp-15-12445-2015, 2015.
- Quinn, P. K., Bates, T. S., Baynard, T., Clarke, A. D., Onasch, T. B., Wang, W., Rood,
- 968 M. J., Andrews, E., Allan, J., Carrico, C. M., Coffman, D., and Worsnop, D.: Impact
- of particulate organic matter on the relative humidity dependence of light scattering: A
- 970 simplified parameterization, Geophys. Res. Lett., 32, 1–4,
- 971 https://doi.org/10.1029/2005GL024322, 2005.
- Ren, J., Chen, L., Fan, T., Liu, J., Jiang, S., and Zhang, F.: The NPF Effect on CCN
- Number Concentrations: A Review and Re-Evaluation of Observations From 35 Sites
- 974 Worldwide, Geophys. Res. Lett., 48, 1–12, https://doi.org/10.1029/2021GL095190,
- 975 2021.
- Rosati, B., Isokääntä, S., Christiansen, S., Jensen, M. M., Moosakutty, S. P., De Jonge,
- 977 R. W., Massling, A., Glasius, M., Elm, J., Virtanen, A., and Bilde, M.:

- 978 Hygroscopicity and CCN potential of DMS-derived aerosol particles, Atmos. Chem.
- 979 Phys., 22, 13449–13466, https://doi.org/10.5194/acp-22-13449-2022, 2022.
- 980 Salma, I., Thén, W., Aalto, P., Kerminen, V. M., Kern, A., Barcza, Z., Petäjä, T., and
- Kulmala, M.: Influence of vegetation on occurrence and time distributions of regional
- new aerosol particle formation and growth, Atmos. Chem. Phys., 21, 2861–2880,
- 983 https://doi.org/10.5194/acp-21-2861-2021, 2021.
- 984 Schuster, G. L., Dubovik, O., and Holben, B. N.: Angstrom exponent and bimodal
- 985 aerosol size distributions, J. Geophys. Res. Atmos., 111, 1-14,
- 986 https://doi.org/10.1029/2005JD006328, 2006.
- 987 Shang, D., Hu, M., Tang, L., Fang, X., Liu, Y., Wu, Y., Du, Z., Cai, X., Wu, Z., Lou,
- 988 S., Hallquist, M., Guo, S., and Zhang, Y.: Significant effects of transport on
- 989 nanoparticles during new particle formation events in the atmosphere of Beijing,
- 990 Particuology, 80, 1–10, https://doi.org/10.1016/j.partic.2022.12.006, 2023.
- 991 Sharma, S. and Mujumdar, P.: Increasing frequency and spatial extent of concurrent
- 992 meteorological droughts and heatwaves in India, Sci. Rep., 7, 1–9,
- 993 https://doi.org/10.1038/s41598-017-15896-3, 2017.
- 994 Shen, X. J., Sun, J. Y., Zhang, Y. M., Wehner, B., Nowak, A., Tuch, T., Zhang, X. C.,
- Wang, T. T., Zhou, H. G., Zhang, X. L., Dong, F., Birmili, W., and Wiedensohler, A.:
- 996 First long-term study of particle number size distributions and new particle formation
- events of regional aerosol in the North China Plain, Atmos. Chem. Phys., 11,
- 998 1565–1580, https://doi.org/10.5194/acp-11-1565-2011, 2011.
- 999 Su, Y. W.: The effects of extreme high temperature day off on electricity conservation,
- 1000 Weather. Clim. Soc., 13, 769–782, https://doi.org/10.1175/WCAS-D-20-0176.1, 2021.
- Sun, J., Hermann, M., Weinhold, K., Merkel, M., Birmili, W., Yang, Y., Flentje, H.,
- Ries, L., Couret, C., Elsasser, M., Sohmer, R., Wirtz, K., Meinhardt, F., Schü, M.,
- Bath, O., Hellack, B., Kerminen, V., Kulmala, M., Ma, N., and Wiedensohler, A.:

- 1004 Measurement report: Contribution of atmospheric new particle formation to ultrafine
- particle concentration, cloud condensation nuclei and radiative forcing: Results from
- 1006 five-year observations in Central Europe, Atmos. Chem. Phys., 1–34,
- 1007 https://doi.org/10.5194/acp-24-10667-2024, 2024.
- Sun, X., Sun, Q., Zhou, X., Li, X., Yang, M., Yu, A., and Geng, F.: Heat wave impact
- on mortality in Pudong New Area, China in 2013, Sci. Total Environ., 493, 789–794,
- 1010 https://doi.org/10.1016/j.scitotenv.2014.06.042, 2014.
- 1011 Sun, Y., Song, L., Yin, H., Zhang, X., Stott, P., Zhou, B., and Hu, T.: 20. Human
- influence on the 2015 extreme high temperature events in Western China, Bull. Am.
- 1013 Meteorol. Soc., 97, S102–S106, https://doi.org/10.1175/BAMS-D-16-0158.1, 2016.
- Tan, J., Zheng, Y., Song, G., Kalkstein, L. S., Kalkstein, A. J., and Tang, X.: Heat
- wave impacts on mortality in Shanghai, 1998 and 2003, Int. J. Biometeorol., 51,
- 1016 193–200, https://doi.org/10.1007/s00484-006-0058-3, 2007.
- 1017 Tang, M., Chan, C. K., Li, Y. J., Su, H., Ma, Q., Wu, Z., Zhang, G., Wang, Z., Ge, M.,
- Hu, M., He, H., and Wang, X.: A review of experimental techniques for aerosol
- 1019 hygroscopicity studies, Atmos. Chem. Phys., 19, 12631–12686,
- 1020 https://doi.org/10.5194/acp-19-12631-2019, 2019.
- 1021 Tao, L., Zhou, Z., Tao, J., Zhang, L., Wu, C., Li, J., Yue, D., Wu, Z., Zhang, Z., Yuan,
- 1022 Z., Huang, J., and Wang, B.: High contribution of new particle formation to ultrafine
- particles in four seasons in an urban atmosphere in south China, Sci. Total Environ.,
- 1024 889, https://doi.org/10.1016/j.scitotenv.2023.164202, 2023.
- Teng, M., Liao, H., Burke, P. J., Chen, T., and Zhang, C.: Adaptive responses: the
- effects of temperature levels on residential electricity use in China, Clim. Change, 172,
- 1027 https://doi.org/10.1007/s10584-022-03374-3, 2022.
- Tian, J., Wang, Q., Zhang, Y., Yan, M., Liu, H., Zhang, N., Ran, W., and Cao, J.:
- 1029 Impacts of primary emissions and secondary aerosol formation on air pollution in an

- urban area of China during the COVID-19 lockdown, Environ. Int., 150, 106426,
- 1031 https://doi.org/10.1016/j.envint.2021.106426, 2021.
- 1032 Titos, G., Burgos, M. A., Zieger, P., Alados-Arboledas, L., Baltensperger, U.,
- Jefferson, A., Sherman, J., Weingartner, E., Henzing, B., Luoma, K., O'Dowd, C.,
- 1034 Wiedensohler, A., and Andrews, E.: A global study of hygroscopicity-driven
- light-scattering enhancement in the context of other in situ aerosol optical properties,
- 1036 Atmos. Chem. Phys., 21, 13031–13050, https://doi.org/10.5194/acp-21-13031-2021,
- 1037 2021.
- 1038 Titos, G., Cazorla, A., Zieger, P., Andrews, E., Lyamani, H., Granados-Muñoz, M. J.,
- Olmo, F. J., and Alados-Arboledas, L.: Effect of hygroscopic growth on the aerosol
- light-scattering coefficient: A review of measurements, techniques and error sources,
- 1041 Atmos. Environ., 141, 494–507, https://doi.org/10.1016/j.atmosenv.2016.07.021,
- 1042 2016.
- 1043 Titos, G., Jefferson, A., Sheridan, P. J., Andrews, E., Lyamani, H., Alados-Arboledas,
- L., and Ogren, J. A.: Aerosol light-scattering enhancement due to water uptake during
- 1045 the TCAP campaign, Atmos. Chem. Phys., 14, 7031–7043,
- 1046 https://doi.org/10.5194/acp-14-7031-2014, 2014.
- 1047 Wang, N., Du, Y., Chen, D., Meng, H., Chen, X., Zhou, L., Shi, G., Zhan, Y., Feng,
- 1048 M., Li, W., Chen, M., Li, Z., and Yang, F.: Spatial disparities of ozone pollution in
- the Sichuan Basin spurred by extreme, hot weather, Atmos. Chem. Phys., 24,
- 1050 3029–3042, https://doi.org/10.5194/acp-24-3029-2024, 2024.
- 1051 Wang, Y., Li, Z., Zhang, R., Jin, X., Xu, W., Fan, X., Wu, H., Zhang, F., Sun, Y., Wang,
- 1052 Q., Cribb, M., and Hu, D.: Distinct Ultrafine- and Accumulation-Mode Particle
- 1053 Properties in Clean and Polluted Urban Environments, Geophys. Res. Lett., 46,
- 1054 10918–10925, https://doi.org/10.1029/2019GL084047, 2019.

- 1055 Wang, Z. B., Hu, M., Sun, J. Y., Wu, Z. J., Yue, D. L., Shen, X. J., Zhang, Y. M., Pei,
- 1056 X. Y., Cheng, Y. F., and Wiedensohler, A.: Characteristics of regional new particle
- 1057 formation in urban and regional background environments in the North China Plain,
- 1058 Atmos. Chem. Phys., 13, 12495–12506, https://doi.org/10.5194/acp-13-12495-2013,
- 1059 2013.
- 1060 Wang, Z., Wu, Z., Yue, D., Shang, D., Guo, S., Sun, J., Ding, A., Wang, L., Jiang, J.,
- Guo, H., Gao, J., Cheung, H. C., Morawska, L., Keywood, M., and Hu, M.: New
- particle formation in China: Current knowledge and further directions, Sci. Total
- Environ., 577, 258–266, https://doi.org/10.1016/j.scitotenv.2016.10.177, 2017.
- 1064 Westervelt, D. M., Pierce, J. R., Riipinen, I., Trivitayanurak, W., Hamed, A., Kulmala,
- 1065 M., Laaksonen, A., Decesari, S., and Adams, P. J.: Formation and growth of nucleated
- particles into cloud condensation nuclei: Model-measurement comparison, Atmos.
- 1067 Chem. Phys., 13, 7645–7663, https://doi.org/10.5194/acp-13-7645-2013, 2013.
- Wu, Z. J., Poulain, L., Birmili, W., Größ, J., Niedermeier, N., Wang, Z. B., Herrmann,
- 1069 H., and Wiedensohler, A.: Some insights into the condensing vapors driving new
- particle growth to CCN sizes on the basis of hygroscopicity measurements, Atmos.
- 1071 Chem. Phys., 15, 13071–13083, https://doi.org/10.5194/acp-15-13071-2015, 2015.
- Wu, Z. J., Zheng, J., Shang, D. J., Du, Z. F., Wu, Y. S., Zeng, L. M., Wiedensohler, A.,
- and Hu, M.: Particle hygroscopicity and its link to chemical composition in the urban
- atmosphere of Beijing, China, during summertime, Atmos. Chem. Phys., 16,
- 1075 1123–1138, https://doi.org/10.5194/acp-16-1123-2016, 2016.
- 1076 Xia, C., Sun, J., Hu, X., Shen, X., Zhang, Y., Zhang, S., Wang, J., Liu, Q., Lu, J., Liu,
- 1077 S., and Zhang, X.: Effects of hygroscopicity on aerosol optical properties and direct
- radiative forcing in Beijing: Based on two-year observations, Sci. Total Environ., 857,
- 1079 159233, https://doi.org/10.1016/j.scitotenv.2022.159233, 2023.

- 1080 Xu, W. Y., Zhao, C. S., Ran, L., Deng, Z. Z., Liu, P. F., Ma, N., Lin, W. L., Xu, X. B.,
- 1081 Yan, P., He, X., Yu, J., Liang, W. D., and Chen, L. L.: Characteristics of pollutants and
- their correlation to meteorological conditions at a suburban site in the North China
- 1083 Plain, Atmos. Chem. Phys., 11, 4353–4369, https://doi.org/10.5194/acp-11-4353-2011,
- 1084 2011.
- 1085 Xu, W., Chen, C., Qiu, Y., Xie, C., Chen, Y., Ma, N., Xu, W., Fu, P., Wang, Z., Pan,
- 1086 X., Zhu, J., Ngcg, N. L., and Sun, Y.: Size-resolved characterization of organic
- aerosol in the North China Plain: New insights from high resolution spectral analysis,
- 1088 Environ. Sci. Atmos., 1, 346–358, https://doi.org/10.1039/d1ea00025j, 2021.
- 1089 Xu, W., Kuang, Y., Xu, W., Zhang, Z., Luo, B., Zhang, X., Tao, J., Qiao, H., Liu, L.,
- and Sun, Y.: Hygroscopic growth and activation changed submicron aerosol
- 1091 composition and properties in the North China Plain, Atmos. Chem. Phys., 24,
- 1092 9387–9399, https://doi.org/10.5194/acp-24-9387-2024, 2024.
- 1093 Xue, B., Kuang, Y., Xu, W., and Zhao, P.: Joint increase of aerosol scattering
- efficiency and aerosol hygroscopicity aggravate visibility impairment in the North
- 1095 China Plain, Sci. Total Environ., 839, 141163,
- 1096 https://doi.org/10.1016/j.scitotenv.2022.156279, 2022.
- Yang, P., Feng, Q., Hong, G., Kattawar, G. W., Wiscombe, W. J., Mishchenko, M. I.,
- Dubovik, O., Laszlo, I., and Sokolik, I. N.: Modeling of the scattering and radiative
- 1099 properties of nonspherical dust-like aerosols, J. Aerosol Sci., 38, 995-1014,
- 1100 https://doi.org/10.1016/j.jaerosci.2007.07.001, 2007.
- 1101 Yarragunta, Y., Srivastava, S., Mitra, D., and Chandola, H. C.: Source apportionment
- of carbon monoxide over India: a quantitative analysis using MOZART-4, Environ.
- 1103 Sci. Pollut. Res., 28, 8722–8742, https://doi.org/10.1007/s11356-020-11099-y, 2021.
- 1104 Zhang, L., Sun, J. Y., Shen, X. J., Zhang, Y. M., Che, H., Ma, Q. L., Zhang, Y. W.,
- Zhang, X. Y., and Ogren, J. A.: Observations of relative humidity effects on aerosol

- light scattering in the Yangtze River Delta of China, Atmos. Chem. Phys., 15,
- 1107 8439–8454, https://doi.org/10.5194/acp-15-8439-2015, 2015.
- Zhang, R., Khalizov, A. F., Pagels, J., Zhang, D., Xue, H., and McMurry, P. H.:
- 1109 Variability in morphology, hygroscopicity, and optical properties of soot aerosols
- during atmospheric processing, Proc. Natl. Acad. Sci. U. S. A., 105, 10291–10296,
- 1111 https://doi.org/10.1073/pnas.0804860105, 2008.
- Zhang, R., Khalizov, A., Wang, L., Hu, M., and Xu, W.: Nucleation and growth of
- 1113 nanoparticles in the atmosphere, Chem. Rev., 112, 1957–2011,
- 1114 https://doi.org/10.1021/cr2001756, 2012.
- Zhang, R., Suh, I., Zhao, J., Zhang, D., Fortner, E. C., Tie, X., Molina, L. T., and
- 1116 Molina, M. J.: Atmospheric new particle formation enhanced by organic acids,
- 1117 Science (80-.)., 304, 1487–1490, https://doi.org/10.1126/science.1095139, 2004.
- Zhang, R., Wang, G., Guo, S., Zamora, M. L., Ying, Q., Lin, Y., Wang, W., Hu, M.,
- and Wang, Y.: Formation of Urban Fine Particulate Matter, Chem. Rev., 115,
- 3803–3855, https://doi.org/10.1021/acs.chemrev.5b00067, 2015.
- 1121 Zhang, Z., Xu, W., Zeng, S., Liu, Y., Liu, T., Zhang, Y., Du, A., Li, Y., Zhang, N.,
- Wang, J., Aruffo, E., Han, P., Li, J., Wang, Z., and Sun, Y.: Secondary Organic
- 1123 Aerosol Formation from Ambient Air in Summer in Urban Beijing: Contribution of
- 1124 S/IVOCs and Impacts of Heat Waves, Environ. Sci. Technol. Lett.,
- https://doi.org/10.1021/acs.estlett.4c00415, 2024.
- Zhao, C., Yu, Y., Kuang, Y., Tao, J., and Zhao, G.: Recent Progress of Aerosol
- 1127 Light-scattering Enhancement Factor Studies in China, Adv. Atmos. Sci., 36,
- 1128 1015–1026, https://doi.org/10.1007/s00376-019-8248-1, 2019.
- Zhao, S., Yu, Y., Li, J., Yin, D., Qi, S., and Qin, D.: Response of particle number
- 1130 concentrations to the clean air action plan: Lessons from the first long-term aerosol

- measurements in a typical urban valley in western China, Atmos. Chem. Phys., 21,
- 1132 14959–14981, https://doi.org/10.5194/acp-21-14959-2021, 2021.
- 1133 Zhu, Y., Shen, Y., Li, K., Meng, H., Sun, Y., Yao, X., Gao, H., Xue, L., and Wang, W.:
- 1134 Investigation of Particle Number Concentrations and New Particle Formation With
- Largely Reduced Air Pollutant Emissions at a Coastal Semi-Urban Site in Northern
- 1136 China, J. Geophys. Res. Atmos., 126, 1-20, https://doi.org/10.1029/2021JD035419,
- 1137 2021.
- Zieger, P., Weingartner, E., Henzing, J., Moerman, M., De Leeuw, G., Mikkilä, J., Ehn,
- 1139 M., Petäjä, T., Clémer, K., Van Roozendael, M., Yilmaz, S., Frieß, U., Irie, H., Wagner,
- 1140 T., Shaiganfar, R., Beirle, S., Apituley, A., Wilson, K., and Baltensperger, U.:
- 1141 Comparison of ambient aerosol extinction coefficients obtained from in-situ,
- 1142 MAX-DOAS and LIDAR measurements at Cabauw, Atmos. Chem. Phys., 11,
- 2603–2624, https://doi.org/10.5194/acp-11-2603-2011, 2011.